5-2016

Vibration Analysis of a Composite Wing Box with Arbitrarily Shaped Spars and Ribs

Rossana R. Fernandes

VIBRATION ANALYSIS OF A COMPOSITE WING BOX WITH ARBITRARILY SHAPED SPARS AND RIBS

A Thesis

Submitted to the Faculty

of

Embry-Riddle Aeronautical University

by

Rossana R. Fernandes

In Partial Fulfillment of the

Requirements for the Degree

of

Master of Science in Aerospace Engineering

May 2016

Embry-Riddle Aeronautical University

Daytona Beach, Florida

VIBRATION ANALYSIS OF A COMPOSITE WING BOX WITH ARBITRARILY SHAPED SPARS AND RIBS

by

Rossana R. Fernandes

A Thesis prepared under the direction of the candidate's committee chairman, Dr. Ali Tamijani, Department of Aerospace Engineering, and has been approved by the members of the thesis committee. It was submitted to the School of Graduate Studies and Research and was accepted in partial fulfillment of the requirements for the degree of Master of Science in Aerospace Engineering.

THESIS COMMITTEE

Chairman, Dr. Ali Tamijani

Member, Dr. Habib Eslami

Member, Dr. Frank Radosta

Department Chair, Dr. Anastasios Lyrintzis
or Graduate Program Coordinator, Dr. Eric Perrell

21 April 2016
Date

Dean of College of Engineering, Dr. Maj Mirmirani

04/21/14
Date

Vice Chancellor, Academic Support, Dr. Christopher Grant

4/22/16
Date

ACKNOWLEDGMENTS

First of all, I would like to thank God for His indisputable presence in my life, for always illuminating my path and for making this thesis possible.

I would like to express my sincere gratitude to my thesis advisor, Dr. Ali Tamijani, for his guidance and encouragement throughout my research. His experience and achievements as a researcher have deeply inspired me and my career path.

I would like to thank my thesis committee for their time and effort in revising my work and participating in my thesis defense. I also thank Dr. Frank Radosta for supporting my master's degree application.

I am eternally grateful to my beloved parents and sister for their love and moral support throughout my life. I also thank my parents for their efforts in providing me and my sister with good values and education. Without them, I could not have completed this thesis.

I would like to thank all of my former professors and instructors for their important and unforgettable contribution to my personal and professional life.

Last but not least, I acknowledge the assistance of the friendly ERAU Hunt library staff in promptly obtaining the articles and books requested.

TABLE OF CONTENTS

LIST OF TABLES

LIST OF FIGURES

SYMBOLS

a	wing semi-span or length of the plate
A_{ij}	element of the extensional stiffness matrix of the plate
A_{sij}	element of the extensional stiffness matrix of the stiffener
b	wing chord or width of the plate
b_s	thickness of the stiffener
B_{ij}	element of the bending-stretching coupling matrix of the plate
B_{sij}	element of the bending-stretching coupling matrix of the stiffener
D_A	aerodynamic damping matrix
D_{ij}	element of the flexural stiffness matrix of the plate
D_{sij}	element of the flexural stiffness matrix of the stiffener
$\overline{D}_p$	flexural rigidity of isotropic plates
D_p	plate's material coefficient matrix
D_s	stiffener's material coefficient matrix
e	distance along the z direction between the plate coordinate system and the global coordinate system.
E_1, E_2	longitudinal and transverse Young's modulus, respectively
F_A	aerodynamic load matrix
g_T	aerodynamic damping parameter
G_{12}, G_{13}, G_{23}	shear modulus of a lamina with respect to the 1, 2 and 3 axes
h_p	plate's thickness
h_s	stiffener's height
I	identity matrix
$\lvert J \rvert$	determinant of the Jacobian of the plate
$\lvert J_s \rvert$	determinant of the Jacobian of the stiffener
k_G^2	shear correction factor
K_p	plate's stiffness matrix
K_s	stiffener's stiffness matrix
L_i	shape function of the stiffener
M_∞	freestream Mach number
M_p	plate's mass matrix
M_s	stiffener's mass matrix
N_i	shape function of the plate
Δp	aerodynamic pressure
q	harmonic solution

$\bar{Q}_{ij}$	element of the transformed reduced stiffness matrix
$1/R$	stiffener's curvature in the $x-y$ plane
t	time
T_p	plate's kinetic energy
T_s	stiffener's kinetic energy
u	plate displacement in the *x* direction
u_0	plate middle surface displacement in the *x* direction
u_s	matrix containing the stiffener's displacement
u_t	stiffener displacement along the tangential direction
U_∞	airstream speed
U_p	plate's strain energy
U_s	stiffener's strain energy
x_i, y_i	x and y coordinates of the i^{th} vertex of the plate, respectively
v	plate displacement in the y direction
v_0	plate middle surface displacement in the y direction
v_n	stiffener displacement along the normal direction
w	out-of-plane displacement of the plate
w_0	out-of-plane displacement of the plate middle surface
w_s	out-of-plane displacement of the stiffener
W_A	work done by aeroelastic forces
α	angle between the stiffener tangential direction and the global x axis
γ_b, γ_n	engineering shear strain of the stiffener in the t, n, b local coordinate system
$\gamma_{xy}, \gamma_{yz}, \gamma_{xz}$	engineering shear strain in the $x-y$, $y-z$ and $x-z$ planes, respectively
Γ	arc length of the stiffener
ε_p	plate strain vector
ε_s	stiffener strain vector
ε_t	stiffener normal strain in the tangential direction
$\varepsilon_x, \varepsilon_y$	normal strains of the plate in the x and y direction, respectively
ζ	natural coordinate of the stiffener
θ_n	rotation about the stiffener tangential direction
θ_t	rotation about the stiffener normal direction
κ_t, κ_n	stiffener bending curvatures in the t and n direction, respectively
κ_x, κ_y	plate bending curvatures in the x and y direction, respectively

κ_{xy}	twisting curvature of the plate
λ	aerodynamic pressure parameter
λ_{cr}	critical aerodynamic pressure parameter
$\nu_{12}, \nu_{13}, \nu_{23}$	Poisson's ratio with respect to the 1, 2 and 3 axes
ξ_i, η_i	coordinates of the i^{th} point of the stiffener in the $\xi - \eta$ plane
ρ	material density
ρ_∞	air density
φ_y	rotation of the plate middle surface about the x axis
φ_x	rotation of the plate middle surface about the y axis
ω	modal frequency
$\overline{\omega}_{cr}$	non-dimensional frequency at the critical dynamic pressure
Ω	eigenvalue
$\Omega_{\mathrm{R}}, \Omega_{\mathrm{I}}$	real and imaginary parts of the eigenvalue, respectively

ABBREVIATIONS

CPU	Central Processing Unit
DLM	Doublet Lattice Method
EBF3	Electronic Beam Freeform Fabrication
FEA	Finite Element Analysis
FEM	Finite Element Methods
FSDT	First Order Shear Deformation Theory
FSW	Friction Stir Welding
GA	Genetic Algorithm
HSDT	High Order Shear Deformation Theory
T.E.	Trailing Edge

ABSTRACT

Fernandes, Rossana R. MSAE, Embry-Riddle Aeronautical University, May 2016. Vibration Analysis of a Composite Wing Box with Arbitrarily Shaped Spars and Ribs.

In this research, the free vibration analysis of composite wing boxes with curvilinear spars and ribs is performed. Modern manufacturing technologies, such as Electron Beam Freeform Fabrication and Friction Stir Welding, have allowed the manufacturing of arbitrarily shaped stiffeners. Curvilinear stiffeners provide flexibility in design as they can assume an infinite number of paths. Curvilinear spars and ribs can in some instances provide a better vibration and static response than their straight counterparts while reducing the overall mass of the structure. An equivalent continuum plate model of a wing box using energy formulations is proposed at the preliminary design stage to reduce the high and costly CPU time incurred from the optimization of finite element models. In the present plate model, the bottom and top skins of the wing box are treated as plates, and the internal structures are treated as beams. The deformations and strains of the model are developed according to the FSDT. The Chebyshev polynomials are the bases of the displacement and rotation functions in the Ritz method. To assess the accuracy and feasibility of the proposed model, several numerical cases of the free vibration and aeroelastic flutter of stiffened panels have been analyzed. The model of a wing box with straight spars and ribs and models with curvilinear spars and ribs made of graphite/epoxy were compared with ANSYS® models. Reasonable agreement has been achieved.

1. Introduction

The current aerospace industry demands innovative designs and materials that offer weight savings, as well as faster and more cost and energy efficient aircraft. To fulfill these needs from the structural point of view, researchers have proposed the use of actuators (Chen et al., 2000), composite materials with curvilinear fibers (Lopes et al., 2008), laminated composite materials, sandwich structures, stiffeners, etc. The present research is first focused on the manipulation of the fiber and stiffener orientations to tailor the dynamic response of laminated composite plates. Subsequently, four different wing boxes are modeled using an equivalent plate model.

1.1. Stiffened Plates

Researchers have demonstrated a strong interest in stiffened structures due to their wide application in aerospace, automotive, shipbuilding and construction. Internal structures offer a high strength-to-weight ratio, improving the response of the structure to buckling, static and dynamic loads. Therefore, stiffeners are often used to tailor the behavior of the structure. The response of a structure can be further enhanced with some weight reduction, in most cases, by using composite materials. To elaborate, using laminated composite materials, the designers have the freedom to tailor the fiber angle for each layer to better meet the operational and loading requirements of the structure.

The literature is rich in papers addressing the static and dynamic behavior of composite plates with straight stiffeners. Kolli and Chandrashekhara (1997) performed a nonlinear transient analysis of composite plates with straight stiffeners. In their study, the plate was treated as a nine-noded isoparametric quadrilateral element, whereas the

stiffeners were represented by a three-noded isoparametric beam element lying along the plate's nodes. Nonlinear deformations were taken into account implementing von Karman nonlinear theory. Kolli and Chandrashekhara (1997) assessed the effects of the height, number, location and lamination scheme of eccentric stiffeners on the deformation of a plate.

Prusty et al. (2001) carried out the failure analysis of composite stiffened plates and shells using the first-ply failure load. The structural model was mathematically developed using finite element analysis (FEA), in which the plate/shell was represented by an eight-noded isoparametric element, and the stiffeners were represented by beam elements. The stress and strain at each node of each lamina were evaluated in order to determine the location of maximum stress. The load at the critical point was progressively increased to assess failure.

In 2005, researchers at Virginia Tech proposed the use of curvilinear stiffeners in place of the conventional straight stiffeners (Kapania et al., 2005). Since then, several papers have been published studying the static, vibration and buckling of isotropic curvilinear stiffened plates through experiments (Tamijani et al., 2010), using FEA (Peng at al., 2015), or variational methods (Tamijani & Kapania, 2010; Tamijani et al., 2010). These publications have demonstrated that the benefits offered by straight stiffeners can sometimes be further enhanced by tailoring the stiffener orientation. Curvilinear stiffeners provide more flexibility in design as they can assume an infinite number of paths. Although not at a commercial level yet, curvilinear stiffened structures have been manufactured owing to emerging methodologies and techniques in manufacturing technologies, such as Electronic Beam Freeform Fabrication (EBF3) and Friction Stir Welding (FSW) (Mulani

et al., 2011). Kapania et al. (2005) explored the effects of the stiffeners orientation, spacing, location and curvature on the buckling of a structure in order to optimize the design. These authors observed that curvilinear stiffeners may lead to structures lighter than straight stiffeners under certain loads.

Tamijani et al. (2010) used the Ritz method to study the free vibration of isotropic plates with curvilinear stiffeners. The plate and stiffeners were modeled according to the first order shear deformation theory (FSDT). Both eccentric and concentric stiffeners were considered. To validate the natural frequency and mode shapes of the curvilinear stiffened plate, an experiment was conducted in which one edge of an aluminum plate was clamped to a table using a steel bracket. The plate was excited by acoustic waves, and the response was sensed using a laser vibrometer. The mathematical model successfully simulated the response of the real plate.

Tamijani et al. (2014) developed a framework that used the meshfree Galerkin's method and Genetic Algorithm (GA) to analyze and optimize the kringing surrogate model of isotropic plates with curvilinear stiffeners. The framework utilized the mass of the stiffened panel as the objective function, the buckling load as the constraint, and the shape and size of the stiffeners as the design variables. These authors compared the results obtained using three approaches: 1) MD.PATRAN®, MD.NASTRAN®, and GA; 2) MD.PATRAN®, MD.NASTRAN®, kringing, and GA; and 3) meshfree, kringing, and GA.

Dang et al. (2010) created a framework to perform a multi-design optimization of straight and curvilinear stiffened panels with cutouts. In their research, a Lockheed Martin panel representative of standard aircraft structures was taken as the baseline design. In this

study, the weight of the stiffened panel was minimized by considering the shape and size of the plate and stiffeners. Constraints on buckling, damage tolerance, stress and crippling were imposed simultaneously.

1.2. Aeroelastic Flutter

Aeroelasticity is a crucial discipline in the design and maintenance of an aircraft. Knowledge in this subject might have prevented incidents, such as the crash of Langley's monoplane in 1903 and of the British Handley Page O/400 twin engine biplane bomber in 1916 (Hirschel et al., 2003). At high speeds, the wing twists and vibrates up and down changing the angle of attack. The change in the angle of attack induces a change of the aerodynamic forces, which subsequently affects the angle of attack, resulting in a continuously vibrating system. The phenomenon of self-excited oscillation of a structure, which extracts energy from the airstream, is called aeroelastic flutter (Flutter, 2005).

Flutter affects elastic structures in a flow and occurs when the structural damping and/or aerodynamic damping are not enough to dissipate the energy absorbed from the flow by the structure (Zhao & Cao, 2013). To increase the flutter speed, designers strive to increase the difference between modal frequencies by increasing the stiffness and changing the mass distribution (Wright & Cooper, 2007). Flutter can also be prevented by eliminating some modes of vibration that cause the phenomenon, through the manipulation of certain design parameters (Chowdary et al., 1996) or through the use of control surfaces and actuators (Foster & Yang, 1998).

As an attempt to improve the future designs and prevent flutter, the literature is rich in papers on the flutter analysis of beams (Moosavi et al., 2005), plates (Chowdary et al.,

1996; Zhao & Cao, 2013) and wings (Alyanak & Pendleton, 2014; Forster & Yang, 1998) of different materials and subjected to different loading conditions. Chowdary, Singha and Parthan (1996) and Singha and Ganapathi (2005) studied the flutter of composite plates. Both studies pointed out a relation between the skew angle, boundary conditions, fiber angle and the flutter behavior of composite panels. Contrary to rectangular panels, the critical dynamic pressure of skew panels decreases as the fiber angle increases from 0° to around 60° and then slightly increases as the fiber angle approaches 90°. For cantilevered isotropic plates, the flutter dynamic pressure decreases as the skew angle increases, whereas for all-edge simply supported or clamped isotropic plates, the increase in the skew angle increases the flutter dynamic pressure. Chowdary et al. (1996) used eight-noded finite element and the linear Piston theory to study flutter in composite skew panels subjected to supersonic flow. They observed that the increase in the panel's aspect ratio increases the flutter boundary.

Ventres and Dowell (1970) studied flutter of plates subjected to a static pressure, in-plane loads and buckling due to thermal load. They used the nonlinear von Karman plate theory to consider nonlinearity and the Galerkin's method to formulate the model of clamped plates in the supersonic regime. The high Mach number aerodynamic theory was used to develop the aerodynamic forces. The theoretical results were compared to previous experiments performed in a wind tunnel.

Koo and Hwang (2004) addressed the impact of structural damping on the flutter characteristics of clamped laminated plates subjected to a supersonic speed. The plate was modeled as a nine-noded isoparametric element. The FSDT, linear Piston theory and Hamilton's principle were used to develop the governing equation of a damped plate. These

authors assumed a hysteretic damping model instead of a viscous damping model since the former is more accurate. They observed that structural damping can stimulate or suppress flutter depending on the fiber orientation. However, structural damping has negligible effect on the critical dynamic pressure when the aerodynamic damping is high.

Flutter of semi-monocoque structures has also been discussed by several researchers (Liao & Sun, 1993; Zhao & Cao, 2013). Liao and Sun (1993) studied the effects of the skew angle, lamination scheme, ply angle as well as the number and location of the stiffeners on the flutter dynamic pressure and frequency of plates and shells. These authors used finite element methods to model an eight-noded shell and plate element, and three-noded beams for the stiffeners. They concluded that the optimal configuration for a stiffened plate would be placing stiffeners parallel to the flow. Placing the stiffeners perpendicular to the flow yielded a system with lower flutter frequency than that of a plate with no stiffeners. Liao and Sun (1993) observed that for an all-edge clamped isotropic stiffened plate, the flutter dynamic pressure and frequency increase as the skew angle increases. Stanford et al. (2014) carried out the aeroelastic topology optimization of metallic blade-stiffened panels. These stiffened panels were discretized into quadrilateral facet-shell finite elements formed by two strain or Kirchhoff triangles. Mode switching in buckling and flutter problems was avoided using two methods: eigenvalue separation constraint and a bound method. Stanford et al. (2014) attempted to hinder local buckling and/or flutter modes by changing the topology of the straight stiffeners.

Several approaches have been applied to address wing flutter. Moosavi et al. (2005) implemented the strip theory and Galerkin's method to estimate the flutter speed and frequency of a subsonic wing. In this research, the wing was approximated as a cantilevered

beam. Hermit-cubic polynomials were used as the trial functions. Moosavi et al. (2005) investigated the effects of flow compressibility on the flutter results. They observed that considering compressible flow reduces the flutter speed and the flutter frequency by 5% and 2.2%, respectively. Alyanak and Pendleton (2014) attempted to improve the aeroelastic performance of a tailless lambda wing by applying the aeroelastic tailoring and active aeroelastic wing design approaches. Eight NASTRAN models of a composite lambda wing with different stiffnesses were created using a MATLAB tool called MstcGeom. The thickness of the skin, spars and ribs, the ply angle and its distribution over the wing were optimized, and the masses and stiffnesses of the eight models were compared. They were able to adjust the composite resistance to bending and torsion caused by maneuvering, while meeting the flutter constraints and failure criteria. By using the proposed approaches, Alyanak and Pendleton (2014) obtained very flexible designs with low conventional control effectiveness while maintaining the vehicle maneuvering.

Control surfaces have been used as an active method of flutter control. Forster and Yang (1998) proposed the use of piezoelectric actuators to overcome flutter of a wing box model in supersonic flow. The wing skin was modeled using an eight-degree-of-freedom quadrilateral membrane element, whereas the spars and ribs were modeled using two-degree-of-freedom bar elements. The first order high Mach number approximation was applied to develop the aerodynamic forces. Actuators were attached to the skin and subjected to an electrical and mechanical load in the axial direction. Non-structural masses were added at the rear spar to place the center of mass between the shear center and the rear spar. The frequency coalescence method was used to determine the flutter speed and was compared with the linear strip theory. The study showed that the flutter speed can be

changed using piezoelectric actuators and in turn changing parameters such as the skin, spar and rib thicknesses.

1.3. Wing Box Models

Designing a wing can be challenging due to its complex details, large number of elements and numerous constraints that make the computation and optimization expensive and difficult. Therefore, equivalent models such as equivalent plate or beam models are often used by researchers and in conceptual design.

Carrera et al. (2012) carried out a free vibration analysis of rectangular, swept and joined isotropic wings using a higher order beam element and FEA. The results were in agreement with those from NASTRAN, and these authors claimed that the method implemented was computationally more efficient than shell and solid modeling.

Kapania and Liu (2000) developed an equivalent plate model of an isotropic sweptback wing with straight spars and ribs. They used Reissner-Mindlin FSDT to model the plate and Legendre polynomials as the interpolation functions in the Ritz Method in place of the simple polynomials used by previous publications. The model was used to carry out the static and vibration analyses of isotropic wings with uniform and non-uniform thickness. The proposed model was in agreement with the FEA.

Vepa (2008) accurately simulated instability of a wing by developing an equivalent plate model of an orthotropic wing. The plate was modeled based on the Reissner-Mindlin FSDT, and the governing equations are a set of Helmholtz equations which were expressed as Hankel functions of the first kind. Vepa (2008) proposed a new integral formulation for the structural model which is coupled with the Doublet Lattice Method (DLM) formulation

to carry out the unsteady aeroelastic analysis of the wing box. The classical Nyquist plot was used to predict the instability points.

Hwu and Tsai (2002) developed a composite sandwich plate model with non-uniform thickness to mathematically represent a multicell wing with spars and ribs. In the referred model, the face of the sandwich structure represented the wing skin and stringers, whereas the core represented the spars and ribs. This model was used to investigate the effects of the wing internal structures (spars and stringers), fiber angle, sweep angle, airfoil shape and warping on the divergence and lift redistribution of the wing. Hwu and Tsai (2002) observed that increasing the number of stringers and spars increases the divergence dynamic pressure but reduces the effective angle of attack.

Locatelli et al. (2014) used a MATLAB-based framework to optimize a supersonic aircraft wing box with curvilinear spars and ribs (SpaRibs) subjected to stress and flutter constraints. These authors attempted to passively control the deformation, increase the load-bearing capabilities and prevent the flutter of the isotropic structure by optimizing the size and shape of the internal elements (spars and ribs). Locatelli et al. (2014) reported a 15% weight reduction by using SpaRibs.

1.4. Scope

The aircraft and spacecraft panels are unavoidably subjected to high frequency oscillations which do not necessarily lead to immediate disaster (Librescu & Silva, 2002) if the panels are properly designed. Therefore, resonance and flutter, among other factors, must be taken into account in order to maximize the performance of a vehicle while keeping the vehicle's weight within allowable limits. Since flight vehicles are mainly formed by

panels and shells with internal structures, such as frames and stringers, it is important to study stiffened shells and panels. This report investigates first the free vibration and aeroelastic characteristics of stiffened panels. The main purpose of this investigation is to validate the present formulations and results for the case of free vibration. The author also aims to uncover the effectiveness of the stiffener's shape and fiber orientation as a passive mechanism for controlling flutter of laminated composite panels at supersonic speeds. Supersonic speeds were considered at this stage of the research for simplicity.

The second part of this report proposes an equivalent plate model based on the energy formulation to study the natural frequencies and mode shapes of composite wing boxes with straight and curvilinear spars and ribs. The proposed model provides a faster and computationally more efficient framework for optimization since it eliminates the need for iterative remeshing required in FEM (Tamijani et al, 2014). To elaborate, the optimization for the shape, size and location of the spars and ribs in an equivalent model would be easily done without modifying the formulation for the skin (Tamijani et al, 2014). The advantage of equivalent modeling over FEM becomes even more prevalent when considering arbitrarily shaped spars and ribs since they can take any shape increasing the complexity and optimization time.

Numerous papers have been published on the free vibration of isotropic wing models with straight spars and ribs. However, to the best of the author's knowledge, there has been no publication addressing the free vibration of composite wing models with arbitrarily shaped spars and ribs. Arbitrarily shaped stiffeners are promising, but before they start being implemented in commercial design, their behavior must be very well understood. This research will certainly enrich the existing knowledge in such types of

structures.

2. Mathematical Formulation

2.1. Strain and Kinetic Energy of the Plate

The proposed wing box is modeled in MATLAB under the assumption that the wing skin behaves like a plate and its internal elements (spars and ribs) behave like beams. This assumption is valid for boxes with small thickness-to-chord ratio (Kapania & Liu, 2000). The plate was modeled with five degrees of freedom (u_0, v_0, w_0, φ_x and φ_y), as depicted in Figure 2.1. The displacements, rotations and strains were developed according to the FSDT:

$$u(x,y,z,t) = u_0(x,y,t) + z\varphi_x(x,y,t)$$

$$v(x,y,z,t) = v_0(x,y,t) + z\varphi_y(x,y,t) \quad (1)$$

$$w(x,y,t) = w_0(x,y,t)$$

The subscript "0" refers to the displacement at the reference plane ($z = 0$) which in this study is taken as the center of the box, i.e., between the top and bottom skin.

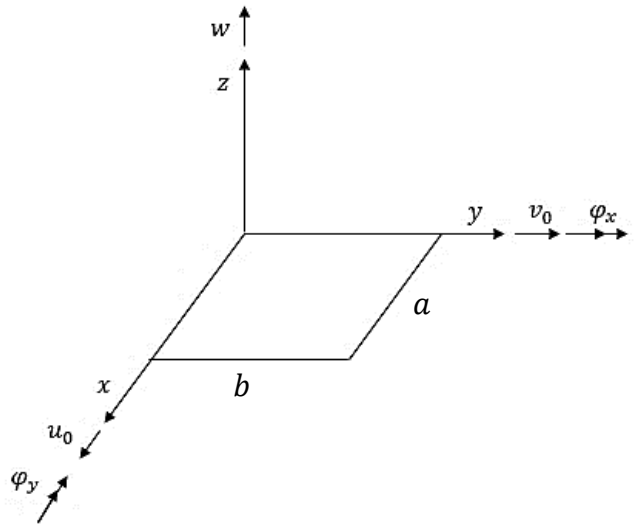

Figure 2.1 Plate midsurface in the global coordinate system

Assuming linear theory, the plate's normal and shear strains are expressed as follows (Tamijani & Kapania, 2010):

$$\varepsilon_p = \begin{Bmatrix} \varepsilon_x \\ \varepsilon_y \\ \gamma_{xy} \\ \kappa_x \\ \kappa_y \\ \kappa_{xy} \\ \gamma_{yz} \\ \gamma_{xz} \end{Bmatrix} = \begin{bmatrix} \frac{\partial u_0}{\partial x} & 0 & 0 & 0 & 0 \\ 0 & \frac{\partial v_0}{\partial y} & 0 & 0 & 0 \\ \frac{\partial u_0}{\partial y} & \frac{\partial v_0}{\partial x} & 0 & 0 & 0 \\ 0 & 0 & \frac{\partial \varphi_x}{\partial x} & 0 & 0 \\ 0 & 0 & 0 & \frac{\partial \varphi_y}{\partial x} & 0 \\ 0 & 0 & \frac{\partial \varphi_x}{\partial y} & \frac{\partial \varphi_y}{\partial x} & 0 \\ 0 & 0 & 0 & \varphi_y & \frac{\partial w_0}{\partial y} \\ 0 & 0 & \varphi_x & 0 & \frac{\partial w_0}{\partial x} \end{bmatrix} \tag{2}$$

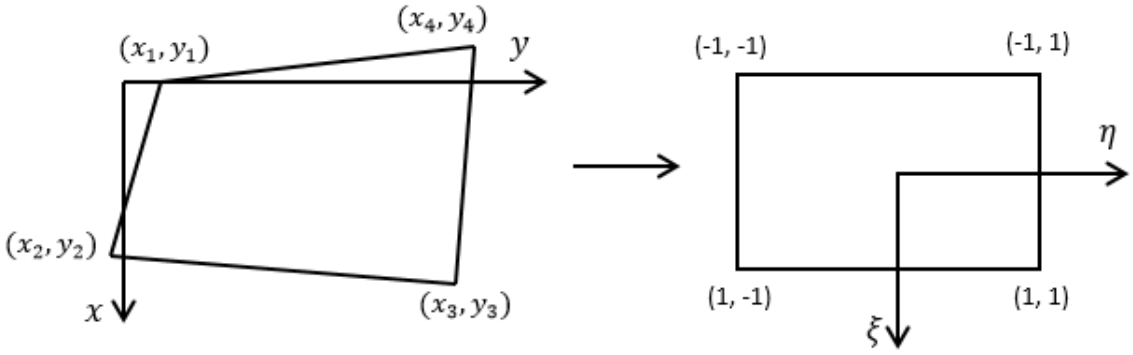

Figure 2.2 Coordinate transformation for the plate

The present formulation considers an arbitrary quadrilateral plate. Therefore, for an easier computation, the plate is mapped into a region (ξ, η) depicted in Figure 2.2 with vertices ranging from -1 to 1, by considering the following transformation (Lovejoy, 1994):

$$x = \sum_{i=1}^{4} N_i(\xi, \eta) x_i$$
$$y = \sum_{i=1}^{4} N_i(\xi, \eta) y_i \tag{3}$$

where (x_i, y_i) are the coordinates of the i^{th} point in the global (x, y, z) coordinate system, and N_i is the shape function defined as follows (Lovejoy, 1994):

$$N_1(\xi, \eta) = \frac{1}{4}(1-\xi)(1-\eta) \qquad N_2(\xi, \eta) = \frac{1}{4}(1+\xi)(1-\eta)$$
$$N_3(\xi, \eta) = \frac{1}{4}(1+\xi)(1+\eta) \qquad N_4(\xi, \eta) = \frac{1}{4}(1-\xi)(1+\eta) \tag{4}$$

The determinant and the inverse of the Jacobian of the transformation are, respectively:

$$|J| = Det\begin{bmatrix} \frac{\partial x}{\partial \xi} & \frac{\partial y}{\partial \xi} \\ \frac{\partial x}{\partial \eta} & \frac{\partial y}{\partial \eta} \end{bmatrix} \tag{5}$$

$$inv(J) = \begin{bmatrix} \frac{\partial \xi}{\partial x} & \frac{\partial \eta}{\partial x} \\ \frac{\partial \xi}{\partial y} & \frac{\partial \eta}{\partial y} \end{bmatrix} = \begin{bmatrix} J_{11} & J_{12} \\ J_{21} & J_{22} \end{bmatrix} \tag{6}$$

Therefore, equation (2) must be applied in the (ξ, η) coordinate system by considering the following relations:

$$\frac{\partial(\,)}{\partial x} = J_{11}\frac{\partial(\,)}{\partial \xi} + J_{12}\frac{\partial(\,)}{\partial \eta}$$
$$\frac{\partial(\,)}{\partial y} = J_{21}\frac{\partial(\,)}{\partial \xi} + J_{22}\frac{\partial(\,)}{\partial \eta} \tag{7}$$

Lovejoy (1994), and Tamijani and Kapania (2010) have demonstrated the accuracy and efficiency of the Chebyshev Polynomials. Therefore, the displacements and rotations were formed by the boundary functions and the Chebyshev polynomials in ξ and η.

$$u_0(\xi,\eta) = \sum_{m=1}^{p}\sum_{n=1}^{q} c_{mn}u_{bx}(\xi,\eta)X_m(\xi)Y_n(\eta)$$
$$v_0(\xi,\eta) = \sum_{m=1}^{p}\sum_{n=1}^{q} d_{mn}v_{by}(\xi,\eta)X_m(\xi)Y_n(\eta)$$
$$\varphi_x(\xi,\eta) = \sum_{m=1}^{p}\sum_{n=1}^{q} e_{mn}\varphi_{bx}(\xi,\eta)X_m(\xi)Y_n(\eta) \tag{8}$$
$$\varphi_y(\xi,\eta) = \sum_{m=1}^{p}\sum_{n=1}^{q} f_{mn}\varphi_{by}(\xi,\eta)X_m(\xi)Y_n(\eta)$$
$$w_0(\xi,\eta) = \sum_{m=1}^{p}\sum_{n=1}^{q} g_{mn}w_{bz}(\xi,\eta)X_m(\xi)Y_n(\eta)$$

where c_{mn}, d_{mn}, e_{mn}, f_{mn} and g_{mn} are the Ritz coefficients. $X_m(\xi)$ and $Y_n(\eta)$ are the Chebyshev polynomials in ξ and η, respectively. $u_{bx(\xi,\eta)}$, $v_{by}(\xi,\eta)$, $\varphi_{bx(\xi,\eta)}$, $\varphi_{by}(\xi,\eta)$ and $w_{bz}(\xi,\eta)$ are functions chosen to satisfy the boundary conditions, as shown:

$$u_{bx(\xi,\eta)} = \left(\frac{\eta+1}{2}\right)^{\alpha_1}\left(\frac{\eta-1}{2}\right)^{\alpha_2}\left(\frac{\xi+1}{2}\right)^{\alpha_3}\left(\frac{\xi-1}{2}\right)^{\alpha_4}$$

$$v_{by(\xi,\eta)} = \left(\frac{\eta+1}{2}\right)^{\beta_1}\left(\frac{\eta-1}{2}\right)^{\beta_2}\left(\frac{\xi+1}{2}\right)^{\beta_3}\left(\frac{\xi-1}{2}\right)^{\beta_4}$$

$$\varphi_{bx(\xi,\eta)} = \left(\frac{\eta+1}{2}\right)^{\iota_1}\left(\frac{\eta-1}{2}\right)^{\iota_2}\left(\frac{\xi+1}{2}\right)^{\iota_3}\left(\frac{\xi-1}{2}\right)^{\iota_4} \quad (9)$$

$$\varphi_{by}(\xi,\eta) = \left(\frac{\eta+1}{2}\right)^{\lambda_1}\left(\frac{\eta-1}{2}\right)^{\lambda_2}\left(\frac{\xi+1}{2}\right)^{\lambda_3}\left(\frac{\xi-1}{2}\right)^{\lambda_4}$$

$$w_{bz}(\xi,\eta) = \left(\frac{\eta+1}{2}\right)^{\vartheta_1}\left(\frac{\eta-1}{2}\right)^{\vartheta_2}\left(\frac{\xi+1}{2}\right)^{\vartheta_3}\left(\frac{\xi-1}{2}\right)^{\vartheta_4}$$

The exponents α_j, β_j, ι_j, λ_j and ϑ_j in equation set (9) determine the boundary conditions at the j^{th} edge of the plate. These exponents are $\alpha_j, \beta_j, \lambda_j, \iota_j, \vartheta_j = 0, 1$ as illustrated in Table 2.1:

Table 2.1. Summary of possible values of the exponents in equation (9)

Exponent	$\boldsymbol{\alpha_j}$	$\boldsymbol{\beta_j}$	$\boldsymbol{\iota_j}$	$\boldsymbol{\lambda_j}$	$\boldsymbol{\vartheta_j}$
0	The edge is free to translate in the x direction.	The edge is free to translate in the y direction.	The edge is free or simply supported in the y direction.	The edge is free or simply supported in the x direction.	The edge is free to translate in the z direction.

Exponent	α_j	β_j	ι_j	λ_j	ϑ_j
1	The edge is clamped or simply supported in the x direction.	The edge is clamped or simply supported in the y direction.	The edge is clamped in the x direction.	The edge is clamped in the y direction.	The edge is clamped or simply supported.

The plate strain energy is the sum of the top and bottom skin, and it is given by:

$$U_p = \frac{1}{2}\sum_{plt=1}^{2}\int_{-1}^{1}\int_{-1}^{1}\left[\varepsilon_p\right]^T\left[D_p\right]_{plt}\left[\varepsilon_p\right]|J|\,d\xi d\eta \tag{10}$$

where the material coefficient matrix, $D_{p_{plt}}$ is (Lovejoy, 1994):

$$D_{p_{plt}} = \begin{bmatrix} A_{11} & A_{12} & A_{16} & \bar{B}_{11} & \bar{B}_{12} & \bar{B}_{16} & 0 & 0 \\ A_{12} & A_{22} & A_{26} & \bar{B}_{12} & \bar{B}_{22} & \bar{B}_{26} & 0 & 0 \\ A_{16} & A_{26} & A_{66} & \bar{B}_{16} & \bar{B}_{26} & \bar{B}_{66} & 0 & 0 \\ \bar{B}_{11} & \bar{B}_{12} & \bar{B}_{16} & \bar{D}_{11} & \bar{D}_{12} & \bar{D}_{16} & 0 & 0 \\ \bar{B}_{12} & \bar{B}_{22} & \bar{B}_{26} & \bar{D}_{12} & \bar{D}_{22} & \bar{D}_{26} & 0 & 0 \\ \bar{B}_{16} & \bar{B}_{26} & \bar{B}_{66} & \bar{D}_{16} & \bar{D}_{26} & \bar{D}_{66} & 0 & 0 \\ 0 & 0 & 0 & 0 & 0 & 0 & k_G^2 A_{44} & k_G^2 A_{45} \\ 0 & 0 & 0 & 0 & 0 & 0 & k_G^2 A_{45} & k_G^2 A_{55} \end{bmatrix} \tag{11}$$

where the matrices $\bar{B}_{\mathrm{ij}}$ and $\bar{D}_{\mathrm{ij}}$ take into account the coordinate translation from the middle surface of the plates' laminate to the global coordinate system of the structure. Therefore, e is the offset distance as shown in Figure 2.3:

$$\bar{B}_{\mathrm{ij}} = B_{ij} + eA_{ij}$$
$$\bar{D}_{\mathrm{ij}} = D_{ij} + 2eB_{ij} + e^2A_{ij} \tag{12}$$

where A_{ij}, B_{ij} and D_{ij} are respectively, the extensional, bending-stretching coupling and flexural stiffness matrices defined as follows:

$$A_{ij} = \sum_{k=1}^{n} \bar{Q}_{ij}{}^{k}(z_{k+1} - z_k) \qquad i,j = 1,2,4,5,6$$
$$B_{ij} = \frac{1}{2}\sum_{k=1}^{n} \bar{Q}_{ij}{}^{k}(z_{k+1}^2 - z_k^2) \qquad i,j = 1,2,6 \tag{13}$$
$$D_{ij} = \frac{1}{3}\sum_{k=1}^{n} \bar{Q}_{ij}{}^{k}(z_{k+1}^3 - z_k^3) \qquad i,j = 1,2,6$$

where $\bar{Q}_{ij}{}^{k}$ are the elements of the transformed reduced stiffness matrix for the k^{th} layer of a total of n layers (Vinson, 2002; Lovejoy, 1994).

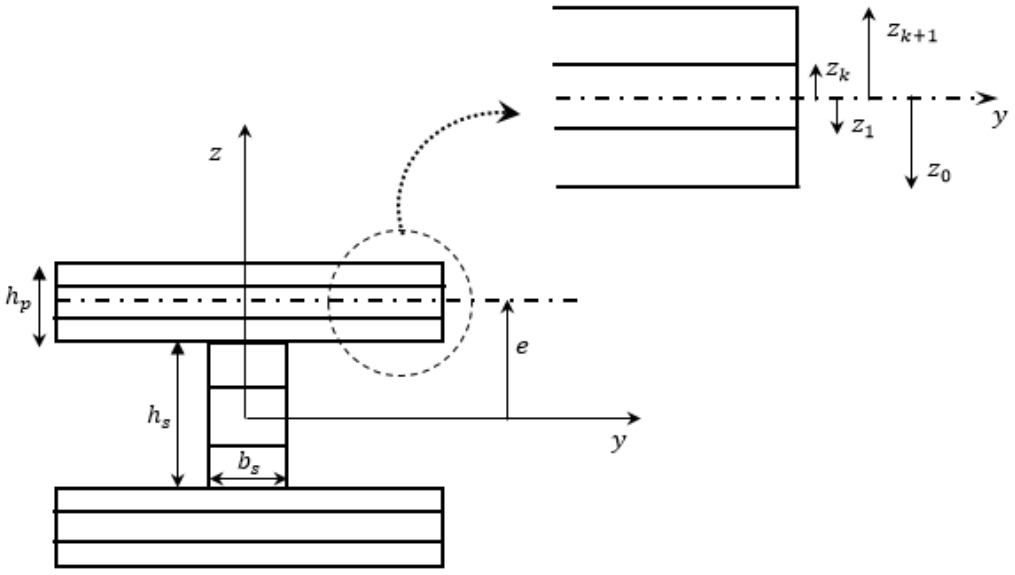

Figure 2.3 $z - y$ plane and layer numbering used for the laminated structure

The shear correction factor, k_G^2, of a laminated plate can be calculated as performed by Vlachoutsis (1992). However, previous publications (Tamijani & Kapania, 2010; Liew et al., 1994) have achieved good accuracy by assuming a constant shear correction factor of $k_G^2 = 5/6$ for a rectangular cross-section which was also assumed in the present research.

Accounting for the top and bottom skin, the total kinetic energy is defined by (Lovejoy, 1994):

$$T_p = \frac{1}{2}\sum_{plt=1}^{2}\int_{-1}^{1}\int_{-1}^{1}\begin{Bmatrix}\dot{u}_0\\ \dot{v}_0\\ \dot{\varphi}_x\\ \dot{\varphi}_y\\ \dot{w}_0\end{Bmatrix}^T\begin{bmatrix}m_1 & 0 & m_2 & 0 & 0\\ 0 & m_1 & 0 & m_2 & 0\\ m_2 & 0 & m_3 & 0 & 0\\ 0 & m_2 & 0 & m_3 & 0\\ 0 & 0 & 0 & 0 & m_1\end{bmatrix}_{plt}\begin{Bmatrix}\dot{u}_0\\ \dot{v}_0\\ \dot{\varphi}_x\\ \dot{\varphi}_y\\ \dot{w}_0\end{Bmatrix}|J|\,d\xi d\eta \tag{14}$$

$$(m_1, m_2, m_3) = \sum_{k=1}^{n}\int_{z_{k-1}+e}^{z_k+e}\rho_k(1, 2z, z^2)dz \tag{15}$$

where the middle surface displacements and rotations are differentiated with respect to time. ρ_k is the density of the k^{th} layer located between $z = z_k$ and $z = z_{k+1}$.

2.2. Strain and Kinetic Energy of the Stiffeners

The stiffeners are modeled with five degrees of freedom and are represented by the line Γ in Figure 2.4. The stiffeners' coordinates are defined as follows:

$$\xi = \sum_{i=1}^{3} L_i(\zeta)\xi_i$$
$$\eta = \sum_{i=1}^{3} L_i(\zeta)\eta_i \tag{16}$$

where $L_i(\zeta)$ and (ξ_i, η_i) are the shape function and the coordinates of the i^{th} point of the stiffeners in the $\xi - \eta$ plane, respectively. The arc length of the stiffeners is defined as follows:

$$\Gamma = \int_{-1}^{1} |J_s| \, d\zeta \tag{17}$$

where the determinant of the Jacobian of the transformation can be defined by (Tamijani & Kapania, 2010):

$$|J_s| = \sqrt{\left(\frac{dx}{d\zeta}\right)^2 + \left(\frac{dy}{d\zeta}\right)^2} \tag{18}$$

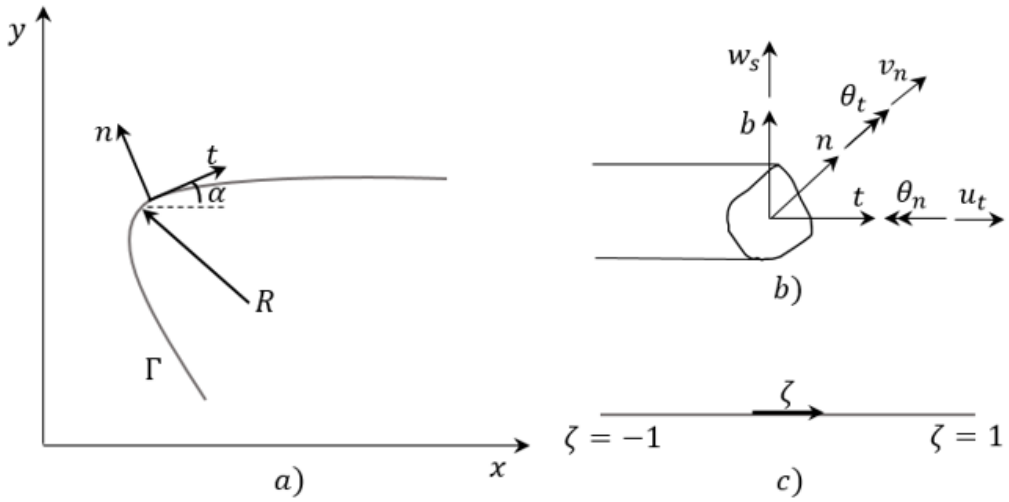

Figure 2.4 Curvilinear Stiffener: a) plate global and stiffener local coordinate systems; b) stiffeners' displacements and rotations; c) stiffeners' natural coordinate system

The stiffeners' curvature is (Tamijani & Kapania, 2010):

$$\frac{1}{R} = \frac{\left(\frac{dx}{d\zeta}\frac{d^2y}{d\zeta^2} - \frac{dy}{d\zeta}\frac{d^2x}{d\zeta^2}\right)}{|J_s|^3} \tag{19}$$

In order to ensure compatibility, the stiffeners' displacements and rotations are expressed in the plate's coordinate system, using the plate's interpolation functions. The total strain energy of the stiffeners is the summation of the strain energy of ns number of stiffeners:

$$U_s = \frac{1}{2}\sum_{st}^{ns}\left(\int_{-1}^{1}[\varepsilon_s]^T[D_s][\varepsilon_s]|J_s|d\zeta\right)_{st} \tag{20}$$

where ε_s is defined by (Tamijani & Kapania, 2010):

$$\varepsilon_s = \begin{Bmatrix}\varepsilon_t\\ \gamma_b\\ \gamma_n\\ \kappa_t\\ \kappa_n\end{Bmatrix} = \begin{bmatrix} \frac{1}{|J_s|}\frac{d}{d\zeta} & \frac{1}{R} & 0 & 0 & 0\\ -\frac{1}{R} & \frac{1}{|J_s|}\frac{d}{d\zeta} & 0 & 0 & 0\\ 0 & 0 & \frac{1}{|J_s|}\frac{d}{d\zeta} & \frac{1}{R} & 0\\ 0 & 0 & -\frac{1}{R} & \frac{1}{|J_s|}\frac{d}{d\zeta} & 0\\ 0 & 0 & 1 & 0 & \frac{1}{|J_s|}\frac{d}{d\zeta} \end{bmatrix}\begin{Bmatrix}u_t\\ v_n\\ \theta_t\\ \theta_n\\ w_s\end{Bmatrix} \tag{21}$$

1/R is the stiffeners' curvature in the $x-y$ plane. Considering layers parallel to the stiffener midsurface, the material coefficient matrix, D_s, is expressed by:

$$D_s = b_s \begin{bmatrix} A_{s11} & A_{s16} & B_{s11} & B_{s16} & 0 \\ A_{s16} & A_{s66} & B_{s16} & B_{s66} & 0 \\ B_{s11} & B_{s16} & D_{s11} & D_{s16} & 0 \\ B_{s16} & B_{s66} & D_{s16} & D_{s66} & 0 \\ 0 & 0 & 0 & 0 & k_G^2 A_{s55} \end{bmatrix} \tag{22}$$

The matrices A_{sij}, B_{sij} and D_{sij} are determined similarly to the previously defined A_{ij}, B_{ij} and D_{ij} matrices. b_s is the thickness of the stiffeners. The total kinetic energy of the stiffeners is given by:

$$T_s = \frac{1}{2} \sum_{st}^{ns} \left(\int_{-1}^{1} [\dot{u}_s]^T [m_s] [\dot{u}_s] |J_s| d\zeta \right)_{st} \tag{23}$$

where the $\dot{u}_s$ indicates the time derivative of the following matrix:

$$[u_s] = \begin{Bmatrix} u_t \\ v_n \\ \theta_t \\ \theta_n \\ w_s \end{Bmatrix} = \begin{bmatrix} \cos\alpha & \sin\alpha & 0 & 0 & 0 \\ -\sin\alpha & \cos\alpha & 0 & 0 & 0 \\ 0 & 0 & \cos\alpha & \sin\alpha & 0 \\ 0 & 0 & -\sin\alpha & \cos\alpha & 0 \\ 0 & 0 & 0 & 0 & 1 \end{bmatrix} \begin{Bmatrix} u_0 \\ v_0 \\ \varphi_x \\ \varphi_y \\ w_0 \end{Bmatrix} \tag{24}$$

α is the angle between the stiffeners' local coordinate system and the global coordinate system, and m_s is:

$$m_s = b_s \begin{bmatrix} m_{s1} & 0 & m_{s2} & 0 & 0 \\ 0 & m_{s1} & 0 & m_{s2} & 0 \\ m_{s2} & 0 & m_{s3} & 0 & 0 \\ 0 & m_{s2} & 0 & m_{s3} & 0 \\ 0 & 0 & 0 & 0 & m_{s1} \end{bmatrix} \tag{25}$$

$$(m_{s1}, m_{s2}, m_{s3}) = \sum_{k=1}^{n} \int_{z_{k-1}}^{z_k} \rho_k (1, z, z^2)\, dz \tag{26}$$

Only eccentric stiffeners have been considered in the present research.

2.3. Aerodynamic Modeling of the Plate

The panel is subject to a supersonic flow on the top and steady air on the bottom (Librescu et al., 2002). Therefore, an air pressure is assumed over the top of the plate along the *x* direction and has no effect on the stiffeners (Liao & Sun, 1993). The work done by the aeroelastic forces is:

$$W_A = \iint_A \Delta p\, w_0\, dA \tag{27}$$

The aerodynamic pressure (Δp) is formulated according to the first-order high Mach number approximation to the linear potential flow theory, as shown (Liao & Sun, 1993):

$$\Delta p = -\lambda \frac{\partial w_0}{\partial x} - g_T \frac{\partial w_0}{\partial t} \tag{28}$$

$$\lambda = \frac{\rho_\infty U_\infty^2}{\sqrt{{M_\infty}^2 - 1}} \tag{29}$$

$$g_T = \frac{\lambda({M_\infty}^2 - 2)}{U_\infty({M_\infty}^2 - 1)} \tag{30}$$

where λ and g_T are the aerodynamic pressure and damping parameters, respectively. M_∞, U_∞ and ρ_∞ are the freestream Mach number, speed and air density, respectively. Assuming that $M_\infty \gg 1$, g_T is approximated as follows (Liao & Sun, 1993):

$$g_T \sim \left(\frac{\mu}{M_\infty}\right)^{0.5} \left(\lambda \frac{\rho h_p}{a}\right)^{0.5} \tag{31}$$

where h_p, a and ρ are the plate's thickness, width and density, respectively, and $\mu = a\rho_\infty/(\rho h_p)$.

2.4. Problem Formulation

By superposition, the kinetic and strain energy of the plates are combined with those of the stiffeners. The numerical integration of the energy equation of the wing box was performed through Gaussian Quadrature. Hamilton's Principle and the Rayleigh-Ritz Method are used to minimize the energy of the structure. Using the Ritz Method the stiffeners can be placed anywhere in the plate without having to lie them along the plate's nodes as imposed in FEA (Tamijani et al., 2010). Neglecting the structural damping and assuming a harmonic solution, the problem can be represented by the following equation (Singha & Ganapathi, 2005):

$$\left\{\ddot{q}\left(M_p + M_s\right) + \dot{q} g_T D_A + q\left(K_p + K_s + \lambda F_A\right)\right\} = 0 \tag{32}$$

where M, K, D_A and F_A are the mass, stiffness, aerodynamic damping and aerodynamic load matrices, respectively. The subscripts p and s stand for plate and stiffener, respectively. When the airflow speed is zero, the problem is reduced to a free-vibration

problem. Since D_A is not proportional to $M_p + M_s$, equation (32) cannot be treated as a simple eigenvalue problem. Instead, it is transformed into the state space configuration (Wright & Cooper, 2007):

$$\begin{Bmatrix}\dot{q}\\ \ddot{q}\end{Bmatrix} - \begin{bmatrix}0 & I\\ -M^{-1}K & -M^{-1}g_T D_A\end{bmatrix}\begin{Bmatrix}q\\ \dot{q}\end{Bmatrix} = 0 \tag{33}$$

where $K = K_p + K_s + \lambda F_A$, $M = M_p + M_s$ and I is the identity matrix. Assuming a harmonic solution, $q = q_0 e^{-i\Omega t}$, where q_0 is a constant, the problem is reduced to an eigenvalue problem for which the eigenvalue $\Omega = \Omega_R \pm i\Omega_I$ and the frequency $\omega = \sqrt{{\Omega_R}^2 + {\Omega_I}^2}$:

$$I\Omega - Q = 0 \tag{34}$$

$$Q = \begin{bmatrix}0 & I\\ -M^{-1}K & -M^{-1}g_T D_A\end{bmatrix} \tag{35}$$

The plots of frequency versus dynamic pressure and damping versus dynamic pressure are generated by solving equation (34) at different dynamic pressures. For the case of the undamped oscillations, flutter occurs when two frequencies coalesce. In other words, as the speed increases, two modal frequencies converge towards each other, since the system is absorbing energy from the airstream (Zhao & Cao, 2013). Hence, the critical dynamic pressure, λ_{cr}, is the one at which two modes first coalesce. However, this is not always the case for more realistic applications in which damping is included. For damped systems, flutter occurs when the real part of the complex eigenvalues (Ω_R) becomes positive (Wright & Cooper, 2007).

For isotropic materials, unless otherwise stated, the aerodynamic pressure parameter and frequency are normalized as follows (Singha & Ganapathi, 2005):

$$\bar{\lambda} = \frac{\lambda a^3}{\bar{D}_p} \tag{36}$$

$$\bar{\omega} = \omega a^2 \left(\frac{\rho h_p}{\bar{D}_p}\right)^{0.5} \tag{37}$$

where $\bar{D}_p$ is the plate's flexural rigidity. For laminated composites, the aerodynamic pressure parameter and frequency are normalized by:

$$\bar{\lambda} = \frac{\lambda a^3}{E_2 h_p^3} \tag{38}$$

$$\bar{\omega} = \frac{\omega a^2}{\pi^2 h_p}\left(\frac{\rho}{E_2}\right)^{0.5} \tag{39}$$

where E_2 is the transverse Young's modulus.

3. Results and Analysis

Several cases are analyzed in this section to validate the presented formulation and gain some insight into the free vibration and flutter of laminated stiffened plates. At last, four wing boxes are modeled. For all of the cases studied, the stiffeners have a rectangular cross-section and are made of the same material as the plate. Also, the plates and stiffeners are modeled using SHELL181 in ANSYS®. The 15th order Chebyshev polynomial was used since it led to a good convergence.

3.1. Free Vibration of Laminated Composite Stiffened Plates

All of the stiffened plates in this subsection are made of a three-layer [45°/-45°/45°] laminated composite material with the following mechanical properties: $E_1 = 60.7\ GPa$, $E_2 = 24.8\ GPa$, $G_{12} = G_{13} = 11.99\ GPa$, $G_{23} = 9.71\ GPa$, $\nu_{12} = \nu_{13} = \nu_{23} = 0.23$ and $\rho = 2550\,\frac{kg}{m^3}$.

3.1.1. Vibration of Straight Stiffened Plates

To assess the accuracy of the present formulation, the author proposes the study of free vibration of the two all-edge clamped composite plates with straight stiffeners represented in Figure 3.1. These square plates have the following common dimensions: $a = b = 1\ m$, $h_p = 6\ mm$, $h_s = 22.4\ mm$ and $b_s = 12.7\ mm$, where a, b and h_p are the plate's length, width and thickness, respectively, and h_s and b_s are the stiffeners' height and thickness, respectively.

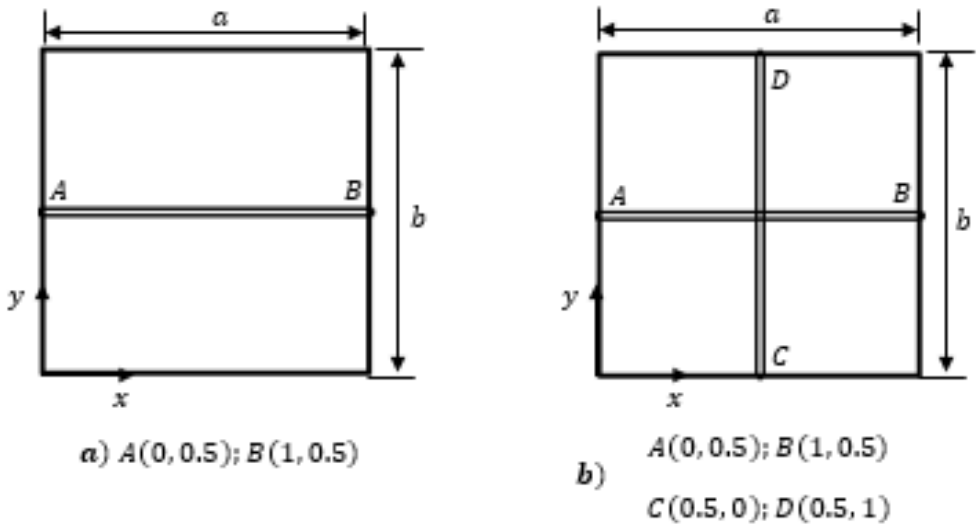

Figure 3.1 Geometric representation of straight stiffened plates

Table 3.1 shows the natural frequencies of the two plates. Good agreement is achieved between the present study and ANSYS® as shown by the relatively low % errors. The slight discrepancy between the two results might be due to the warping that is neglected in this study but is considered in ANSYS®.

Table 3.1 Natural frequencies of C-C-C-C three-layered [45°/-45°/45°] stiffened plates

	Figure 3.1-*a*			**Figure 3.1-*b***		
Mode	**Present**	**ANSYS**	**% Error**	**Present**	**ANSYS**	**% Error**
1	67.10	63.65	5.42	87.29	81.59	6.99
2	90.15	80.71	11.70	122.57	126.82	3.35
3	125.79	121.53	3.51	125.23	127.28	1.61

	Figure 3.1-a			Figure 3.1-b		
Mode	**Present**	**ANSYS**	**% Error**	**Present**	**ANSYS**	**% Error**
4	131.40	122.21	7.52	128.14	127.99	0.12
5	147.51	143.46	2.82	171.79	171.12	0.39
6	187.34	181.23	3.37	217.78	226.35	3.79
7	189.38	183.62	3.14	248.99	257.72	3.39
8	232.56	223.95	3.84	260.45	276.82	5.91
9	242.03	225.46	7.35	287.83	290.85	1.04
10	266.14	259.66	2.50	329.40	330.09	0.21

3.1.2. Vibration of Curvilinearly Stiffened Plates

Table 3.2 shows the natural frequencies for the two curvilinearly stiffened plates of Figure 3.2 with all-edge simply supported. The mode shapes of the plate in Figure 3.2-b are shown in Table 3.3. These two stiffened plates have the following common geometry: $a = 0.6069\ m$, $b = 0.7112\ m$, $h_p = 6.25\ mm$, $h_s = 22.4\ mm$ and $b_s = 4.06\ mm$.

The results have been successfully validated. Table 3.1 and Table 3.2 show that two stiffeners have a better response than one stiffener, as expected, since the stiffeners make the structure stiffer. This effect is more evident for higher vibration modes.

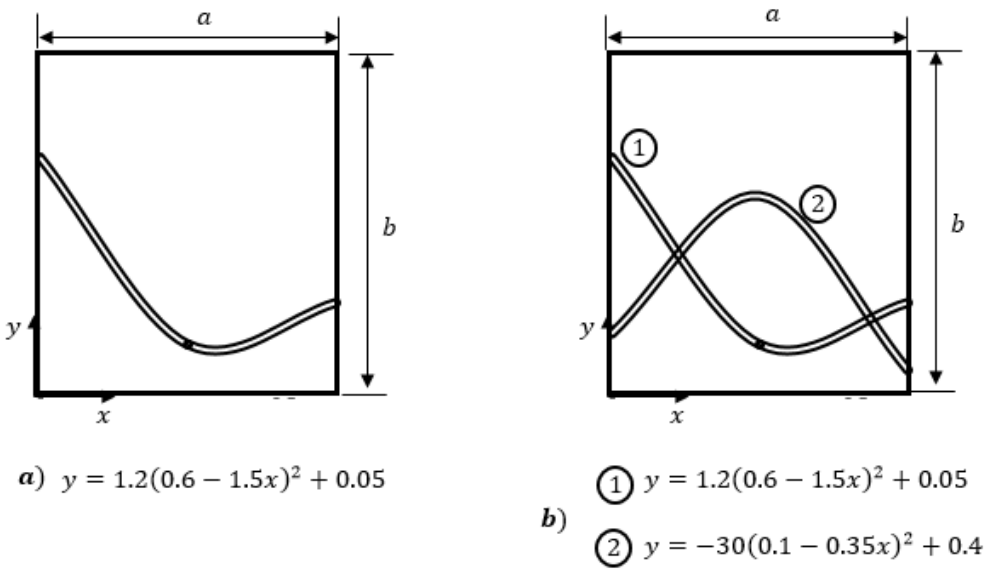

Figure 3.2 Geometric representation of the curvilinearly stiffened plates (Tamijani & Kapania, 2010)

Table 3.2 Natural frequencies of S-S-S-S three-layered [45°/-45°/45°] curvilinearly stiffened plates

	Figure 3.2- *a*			**Figure 3.2- *b***		
Mode	**Present**	**ANSYS®**	**% Error**	**Present**	**ANSYS®**	**% Error**
1	59.18	60.93	2.87	70.40	67.18	4.79
2	128.58	133.68	3.82	147.54	147.96	0.28
3	154.38	150.55	2.54	185.39	174.71	6.11
4	226.14	230.18	1.76	251.03	249.62	0.56
5	249.30	251.11	0.72	263.72	265.26	0.58

	Figure 3.2- a			Figure 3.2- b		
Mode	**Present**	**ANSYS®**	**% Error**	**Present**	**ANSYS®**	**% Error**
6	299.75	291.68	2.77	332.13	328.37	1.15
7	349.16	352.65	0.99	388.40	378.89	2.51
8	389.39	392.24	0.73	415.29	422.14	1.62
9	402.07	403.22	0.29	464.37	442.86	4.86
10	493.01	501.41	1.68	527.08	516.74	2.00

Table 3.3 First three modes of vibration obtained for a plate with two curvilinear stiffeners (Figure 3.2- b)

Present	**ANSYS®**
Mode 1, $\omega = 70.40$	Mode 1, $\omega = 67.18$
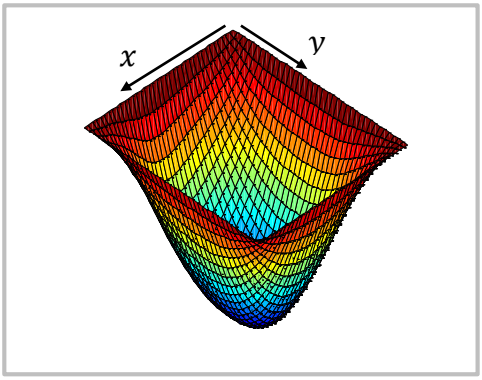	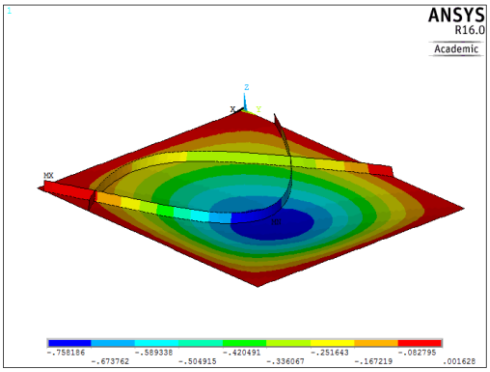
Mode 2, $\omega = 147.54$	Mode 2, $\omega = 147.96$

Present	ANSYS®
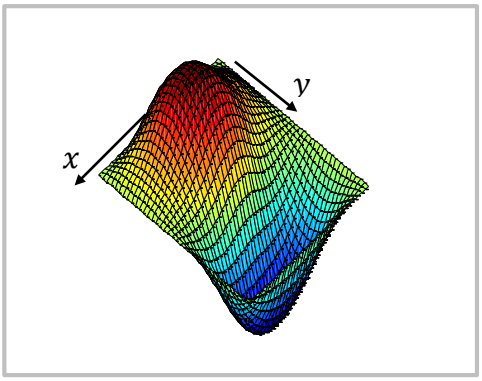	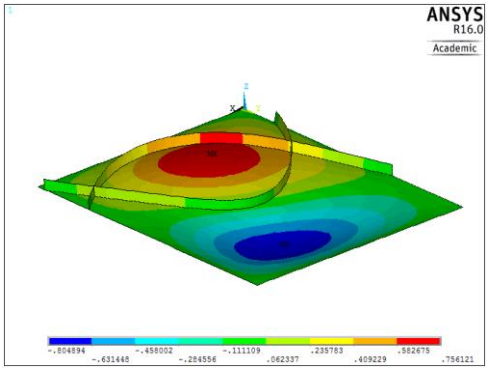
Mode 3, $\omega = 185.39$	Mode 3, $\omega = 174.71$
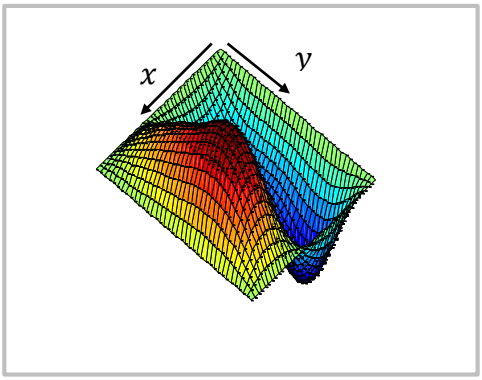	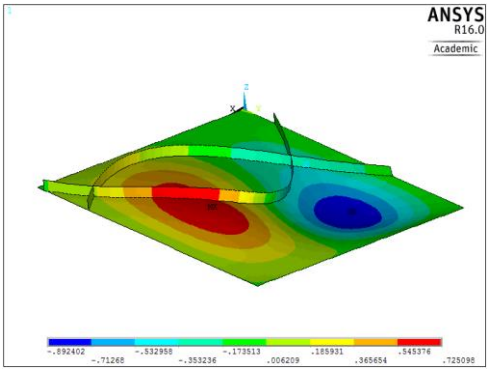

3.1.3. Vibration of Curvilinearly Stiffened Skew Plates

The two C-C-C-C 30° skew plates considered in this section are illustrated in Figure 3.3. These plates have the same dimensions as those in subsection 3.1.1.

The natural frequencies of the two plates and mode shapes of the plate with one curvilinear stiffener (Figure 3.3-a) are shown in Table 3.4 and Table 3.5, respectively. The results have been successfully validated upon comparison with ANSYS®.

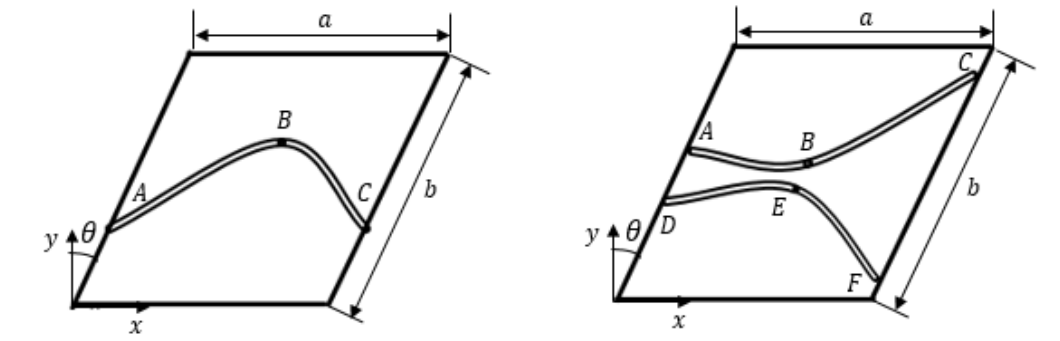

a) $A(0.166, 0.287); B(0.834, 0.579); C(1.165; 0.287)$

b) $A(0.3, 0.520); B(0.775, 0.476); C(1.450, 0.779)$ $D(0.2, 0.346); E(0.725, 0.390); F(1.05, 0.087)$

Figure 3.3 Geometric representation of the curvilinearly stiffened skew plates

Table 3.4 Natural frequencies of C-C-C-C three-layered [45°/-45°/45°] laminate curvilinearly stiffened plates

	Figure 3.3-*a*			**Figure 3.3-*b***		
Mode	**Present**	**ANSYS®**	**% Error**	**Present**	**ANSYS®**	**% Error**
1	68.63	64.93	5.70	86.75	79.07	9.71
2	103.66	104.12	-0.44	123.62	122.55	0.87
3	133.36	132.21	0.87	159.12	164.88	-3.49
4	165.65	157.72	5.03	182.49	174.35	4.67
5	199.33	195.61	1.90	229.55	203.27	12.93
6	212.37	211.04	0.63	265.23	261.29	1.51
7	244.61	230.79	5.99	271.94	278.19	-2.25

	Figure 3.3- a			Figure 3.3-b		
Mode	**Present**	**ANSYS®**	**% Error**	**Present**	**ANSYS®**	**% Error**
8	255.24	270.17	-5.53	320.12	340.05	-5.86
9	280.14	282.30	-0.77	374.04	377.61	-0.95
10	301.85	306.59	-1.55	409.41	403.21	1.54

Table 3.5 First three modes of vibration obtained for a skew plate with one curvilinear stiffener (Figure 3.3- a)

Present	**ANSYS®**
Mode 1, $\omega = 68.63$	Mode 1, $\omega = 64.93$
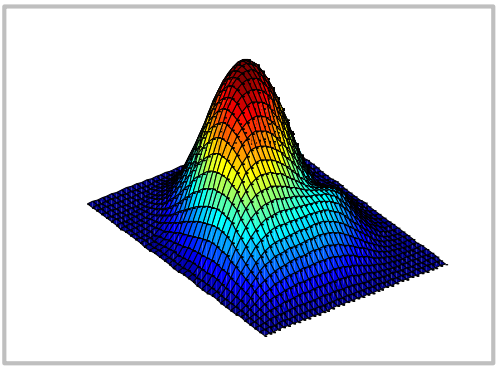	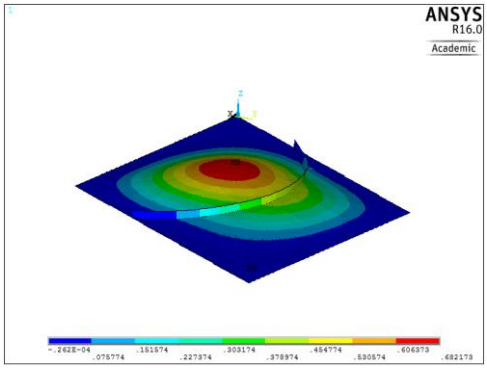
Mode 2, $\omega = 103.66$	Mode 2, $\omega = 104.12$

Present	ANSYS®
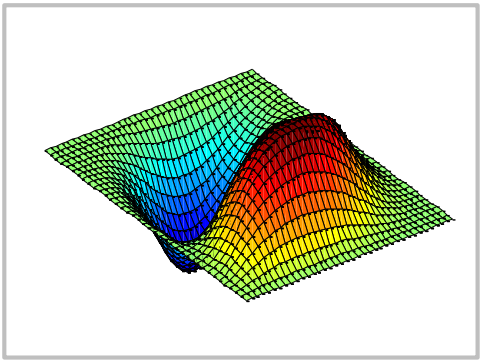	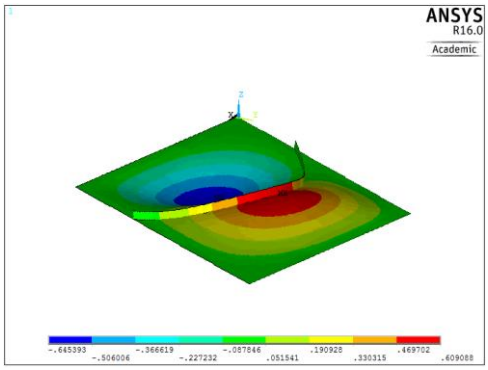
Mode 3, $\omega = 133.36$	Mode 3, $\omega = 132.21$
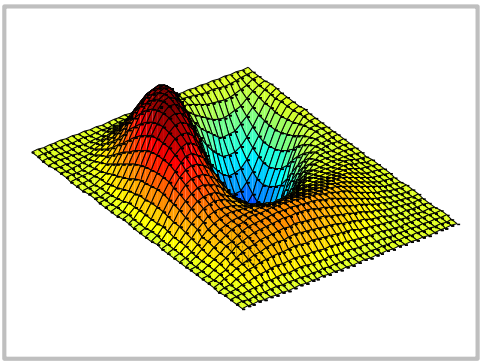	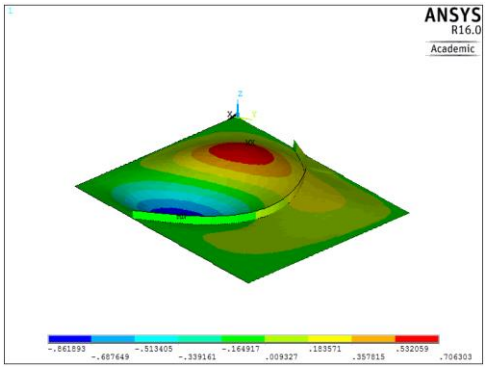

3.2. Aeroelastic Panel Flutter

Designers strive to increase the critical flutter speed in order to prevent flutter. The mode shapes and the plots of frequency versus dynamic pressure and damping versus dynamic pressure are used in this subsection to determine the critical dynamic pressure. Subsections 3.2.1 and 3.2.2 are to validate the present formulation by comparing the results for unstiffened plates and straight stiffened plates with previously published papers (Singha & Ganapathi, 2005; Liao & Sun, 1993). Subsection 3.2.3 analyzes the flutter of laminated rectangular plates with curvilinear stiffeners. Subsection 3.2.4 extends this study to laminated skew plates. Structural damping is beyond the scope of this research.

3.2.1. Flutter of Unstiffened Plates

The main source of validation in this subsection is the work done by Singha and Ganapathi (2005). To be consistent with the referred paper, the aerodynamic damping is neglected, and the coalescence method is used to determine the λ_{cr}. First, the relationship between the skew angle and the critical dynamic pressure is explored. Table 3.6 shows the λ_{cr} for three isotropic thin skew plates ($a = b$ and $a/h_p = 100$) simply supported on all edges. The λ_{cr} is determined from the plot of non-dimensional natural frequencies ($\bar{\omega}$) versus non-dimensional aerodynamic pressure ($\bar{\lambda}$), as shown in Figure 3.4 for the rectangular plate. For the sake of brevity, the plots for the other plates in Table 3.6 are omitted. $\bar{\lambda}_{cr} = \lambda a^3/(D_p \pi^4)$.

Table 3.6 Critical aerodynamic pressure parameter $\bar{\lambda}_{cr} = \lambda a^3/(D_p \pi^4)$ for S-S-S-S isotropic plates

Skew Angle	Present	Singha & Ganapathi, 2005	Liao & Sun, 993
0°	5.24	5.27	5.11
15°	5.48	-----	5.35
30°	6.45	6.47	6.31

Table 3.6 shows that for all-edge simply supported isotropic plates, the critical dynamic pressure increases as the skew angle increases, corroborating the remarks previously made by Liao and Sun (1993). For the three cases in Table 3.6 and for isotropic

plates in general, the critical coalescing mode pair is (1, 2) as depicted in Figure 3.4. The slight discrepancy between the three sets of results in Table 3.6 might be due to the different formulations used by the authors. Singha and Ganapathi (2005) used finite element methods with ten degrees of freedom per node and applied linear polynomials to represent the in-plane displacements and rotations and nonlinear polynomials for the out-of-plane displacement. Liao and Sun (1993) used a three dimensional shell element to model the plate.

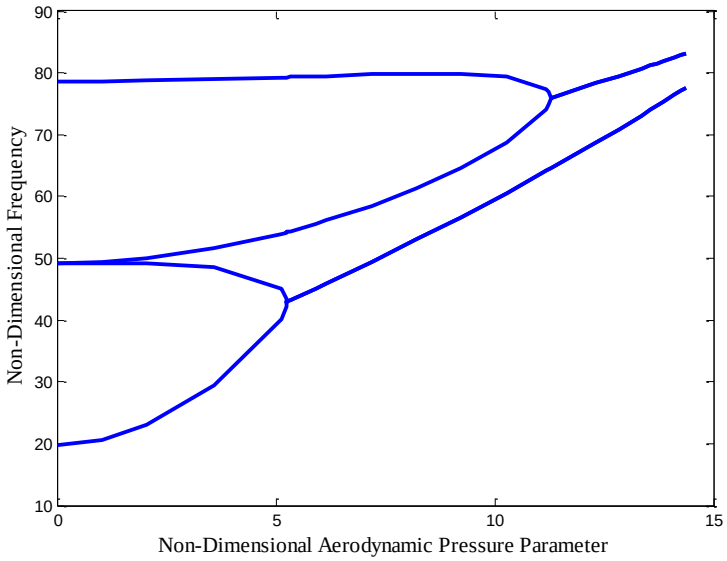

Figure 3.4 $\bar{\omega}$ vs. $\bar{\lambda}/\pi^4$ for the simply supported isotropic rectangular plate

Next, the effect of the skew angle on the critical dynamic speed of laminated composite plates is studied. For this effect, all-edge simply supported [0°/90°/0°/90°/0°] laminated square plates with 0° and 15° skew angle are compared, by plotting the non-dimensional natural frequencies ($\bar{\omega}$) versus non-dimensional aerodynamic pressure ($\bar{\lambda}$). The thin laminates ($a/h_p = 100$) have the following material properties: $E_1/E_2 = 40$, $G_{12}/E_2 = 0.6$, $G_{23}/E_2 = 0.5$, and $\nu_{12} = 0.25$.

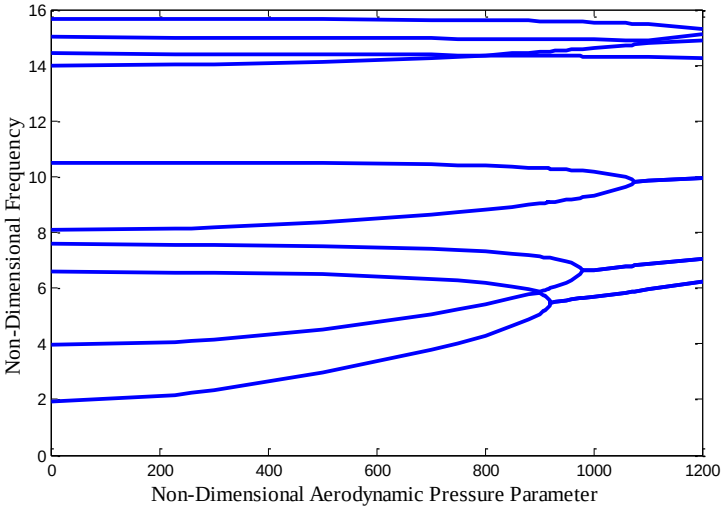

Figure 3.5 $\bar{\omega}$ vs. $\bar{\lambda}$ for a simply supported cross-ply composite plate with 0° skew angle

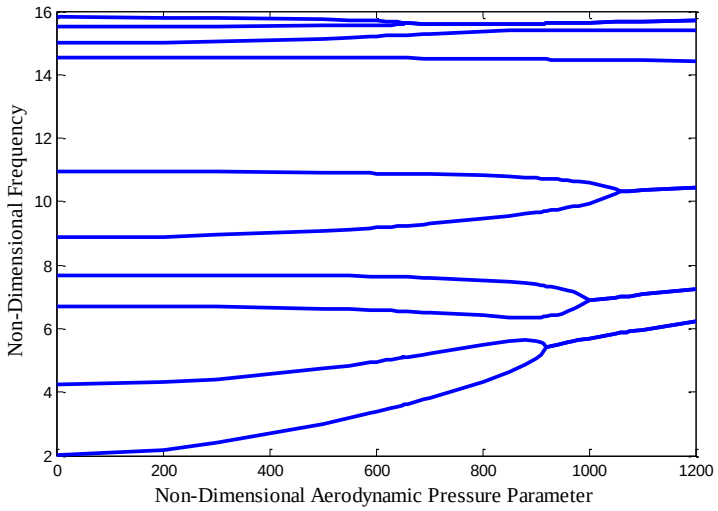

Figure 3.6 $\bar{\omega}$ vs. $\bar{\lambda}$ for a simply supported cross-ply composite plate with 15° skew angle

Figure 3.5 and Figure 3.6 show that the critical coalescing modes of simply supported plates vary with the skew angle in accordance to Singha and Ganapathi (2005). For the 0° skew plate, the critical pair of coalescing modes is (1, 3), whereas for the 15° skew plate, the first pair of coalescing modes is (9, 10). Table 3.7 presents the critical

dynamic pressure of the two cross-ply laminated skew plates for a set of all-edge clamped and all-edge simply supported boundary conditions. Contrary to what is observed for the isotropic cases in Table 3.6, the results in Table 3.7 convey that for laminated plates, the critical dynamic pressure decreases as the skew angle increases. In general, this is only true if the critical mode pair changes with the skew angle, as pointed out by Singha and Ganapathi (2005). The results in this subsection are in good agreement with those obtained by Singha and Ganapathi (2005).

Table 3.7 $\bar{\lambda}_{cr}$ for cross-ply [0°/90°/0°/90°/0°] laminated composite plates

Skew Angle	**Simply Supported**			**Clamped**		
	Present	**Singha & Ganapathi (2005)**	**% Error**	**Present**	**Singha & Ganapathi (2005)**	**% Error**
0°	920.00 (1, 3)	909.50 (1, 3)	1.15	1639.00 (1, 2)	1570.20 (1, 2)	4.38
15°	655.00 (9, 10)	690.60 (9, 10)	5.15	1409.00 (7, 9)	1339.50 (7, 9)	5.19

3.2.2. Flutter of Straight Stiffened Plates

In this subsection, the developed formulation is validated by comparing the results with those provided by Liao and Sun (1993). Unless otherwise stated, thin square isotropic

plates ($a/h_p = 40$, $h_s/h_p = 1.5$, $b_s/a = 0.01$ and $\mu/M_\infty = 0.01$), clamped on all edges, are considered for the different case studies in this subsection. The geometries of the plates are presented in Figure 3.7. Since the aerodynamic damping is taken into account in this and subsequent sections, the λ_{cr} is the smallest λ at which the real part of the eigenvalue (Ω_R) becomes positive.

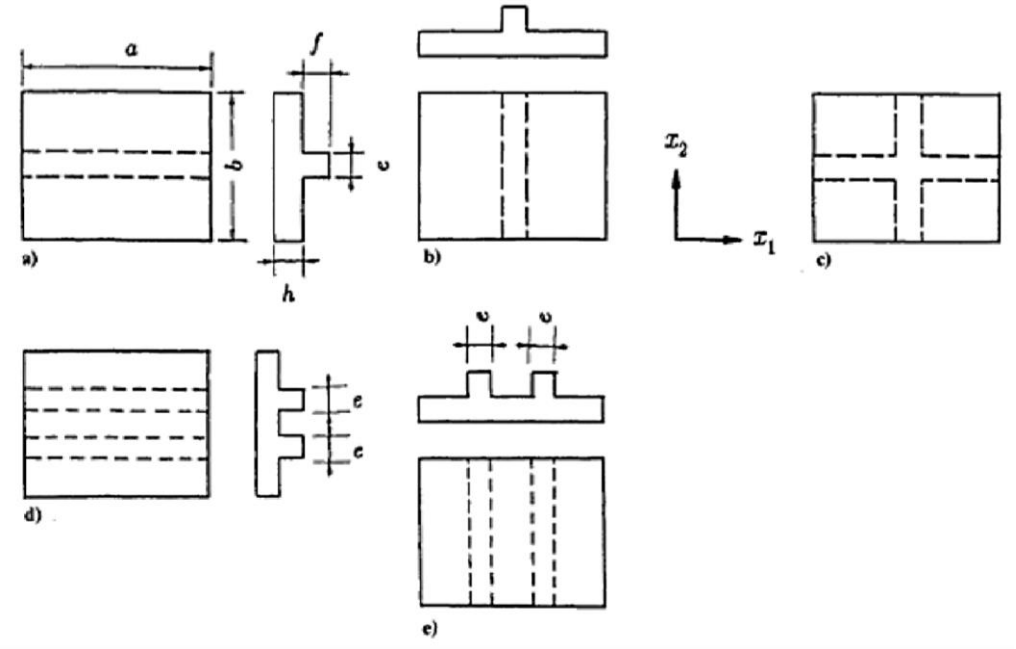

Figure 3.7 Geometry of stiffened plates studied in section III. B (Liao and Sun, 1993).

$$(e = b_s, h = h_p, f = h_s)$$

This section starts by studying the effect of the position and the number of straight stiffeners. First, a single stiffener is placed at the center of the plate parallel ($\parallel$) to the flow (Figure 3.7- a), and then at the center of the plate, but perpendicular ($\perp$) to the flow (Figure 3.7-b). Figure 3.8 and Figure 3.9 show $\bar{\omega}$ vs. $\bar{\lambda}$ and Ω_R vs. $\bar{\lambda}$ plots for the two cases. A plate with two stiffeners parallel (Figure 3.7- d), and normal (Figure 3.7- e) to the flow direction are also studied. The λ_{cr} for these cases are assessed and presented in Table 3.8.

Figure 3.8 shows that placing a single stiffener in the flow direction significantly increases the critical dynamic pressure and flutter speed. On the other hand, a stiffener perpendicular to the flow has a negligible effect on the critical dynamic pressure of the plate, as shown in Figure 3.9. In fact, Liao and Sun (1993) reported that a plate with a perpendicular stiffener has a lower critical dynamic pressure than an unstiffened plate. Also, adding one more stiffener (Figure 3.7- e), in this case, does not significantly increase the critical flutter speed when compared to the unstiffened plate, and a trade study could be investigated with the weight considerations. This is due to the fact that adding one more stiffener causes the adjacent frequencies that form the critical flutter mode to become closer to each other (Liao & Sun, 1993). These remarks are in agreement with those reported in previous studies (Zhao & Cao, 2013; Liao & Sun, 1993).

Table 3.8 indicates that the cross-stiffeners in Figure 3.7-c increase the critical flutter speed of the structure to almost that of a single central stiffener in the direction of the flow, but with increase of weight. Also, the critical coalescing mode pair for all of the cases in Table 3.8 is (1, 2). The discrepancies between the present study and results from Liao and Sun (1993) might be due to the fact that they considered six degrees of freedom to formulate the stiffener's displacements and rotations.

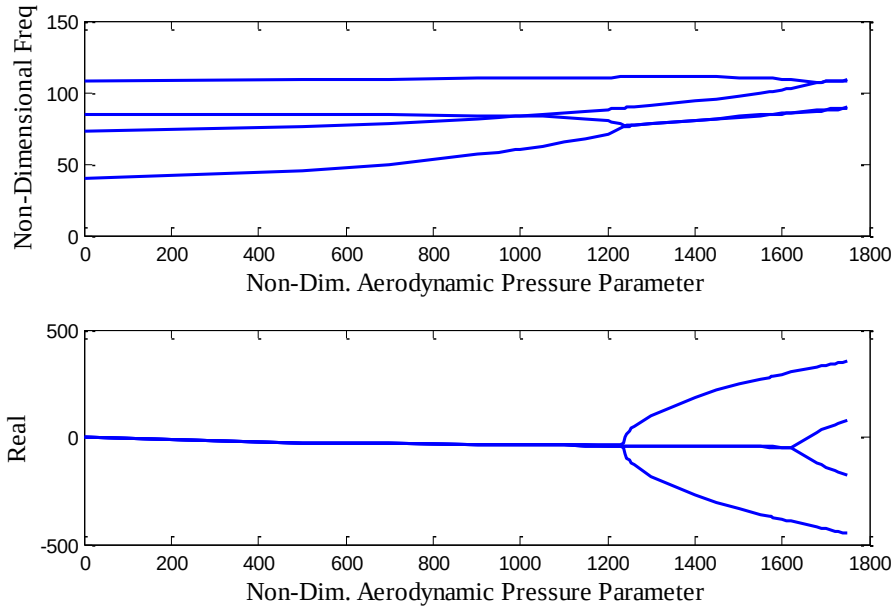

Figure 3.8 $\bar{\omega}$ vs. $\bar{\lambda}$ and Ω_R vs. $\bar{\lambda}$ for an isotropic plate with a central stiffener parallel to the flow

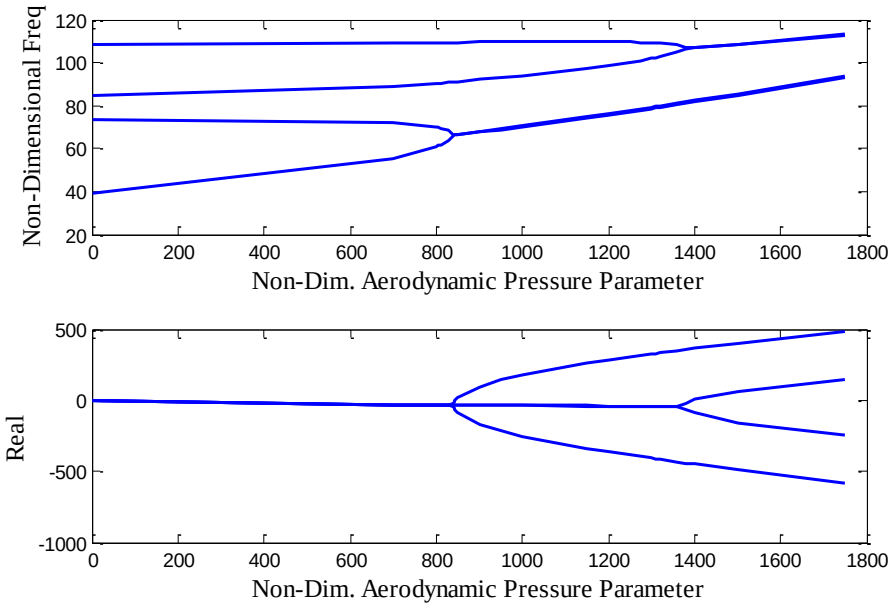

Figure 3.9 $\bar{\omega}$ vs. $\bar{\lambda}$ and Ω_R vs. $\bar{\lambda}$ for an isotropic plate with a central stiffener perpendicular to the flow

Table 3.8 $\bar{\omega}_{cr}$ and $\bar{\lambda}_{cr}$ for C-C-C-C isotropic stiffened square plates

Case Study	$\bar{\omega}_{cr}$			$\bar{\lambda}_{cr}$		
	Present	**Liao & Sun (1993)**	**% Error**	**Present**	**Liao & Sun**	**% Error**
No Stiffener	64.90	65.26	0.55	836.00	867.66	3.65
1 Stiffener ∥ to Flow	76.53	77.23	0.91	1240.00	1315.32	5.73
1 Stiffener ⊥ to Flow	66.20	65.87	0.50	843.30	840.72	0.31
2 Stiffener ∥ to Flow	79.59	79.66	0.09	1383.00	1434.21	3.57
2 Stiffener ⊥ to Flow	67.43	67.36	0.10	860.30	859.47	0.10
Cross Stiffeners	77.12	73.54	4.87	1249.60	1172.72	6.56

3.2.3. Flutter of Curvilinearly Stiffened Plates

Several laminated square plates with stiffeners of different orientations and locations are considered in this section in order to assess the efficiency of curvilinear stiffeners in preventing flutter. The stiffened plates have the following common dimensions: $a = b = 1\ m$, $h_p = 6\ mm$, $h_s = 22.4\ mm$ and $b_s = 12.7\ mm$. Aerodynamic

damping is considered in this section (μ/M_∞ = 0.01).Previous studies have shown that the stiffener location plays a significant role in the flutter behavior of a plate (Singha & Ganapathi, 2005), and so does the material (Alyanak & Pendleton, 2014). Therefore, each of the stiffened plate configurations is analyzed for five different laminates with the following properties: $E_1 = 60.7\ GPa$, $E_2 = 24.8\ GPa$, $G_{12} = 11.99\ GPa$, $G_{13} = 11.99\ GPa$, $G_{23} = 9.71\ GPa$, $\nu_{12} = \nu_{23} = \nu_{13} = 0.23$ and $\rho = 2550\frac{kg}{m^3}$. Figure 3.10 shows the four main stiffened plates studied in this section.

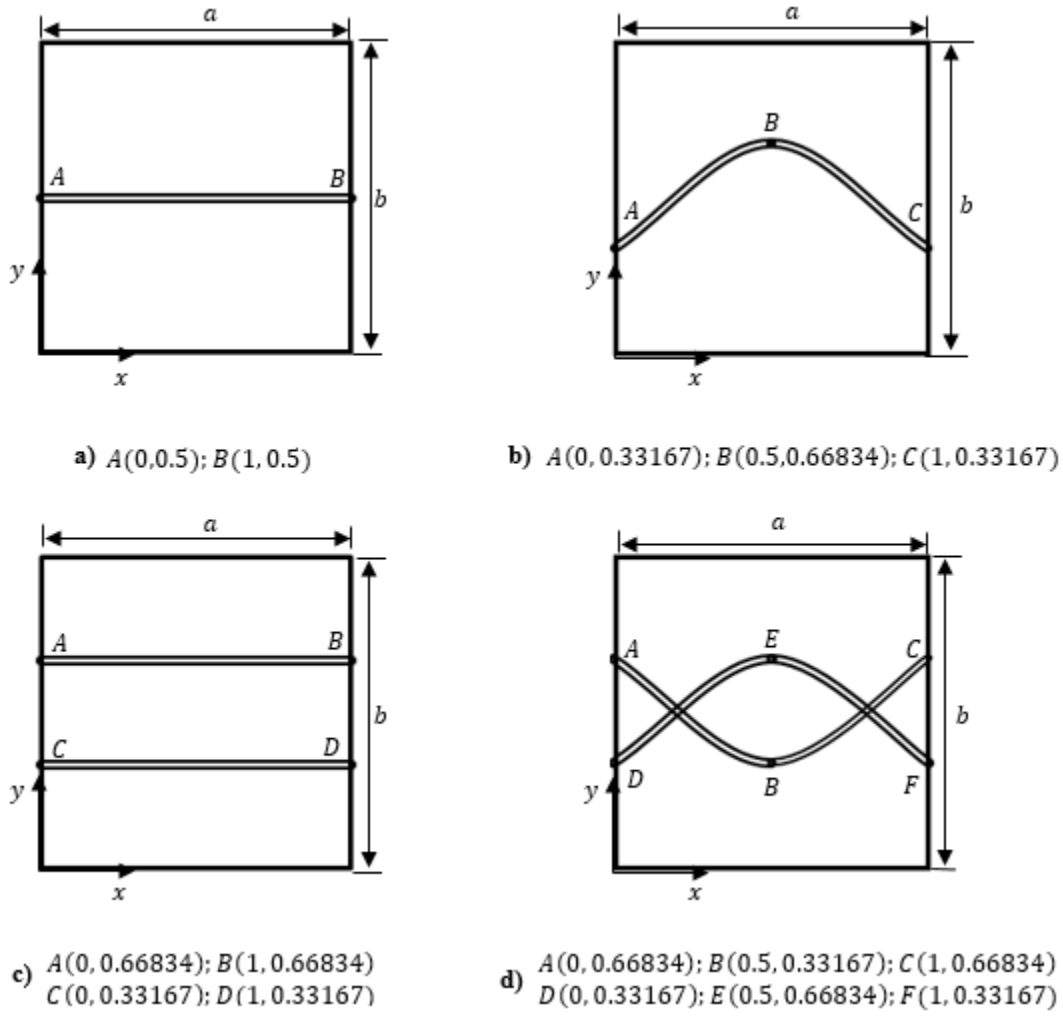

Figure 3.10 Schematic representation of the four stiffener's configuration studied in this section

The plots of $\bar{\omega}$ vs. $\bar{\lambda}$ and Ω_R vs. $\bar{\lambda}$ are generated to determine the critical dynamic pressure for each of the case studies in Figure 3.10. In this section, these characteristic plots are obtained by considering the first twenty frequencies. Figure 3.11 illustrates the plots for the case represented in Figure 3.10- b. The plots for the remaining cases are omitted for sake of brevity. Figure 3.11 shows that the first coalescing modes are mode (2, 3), and $\bar{\lambda}_{cr} = 151.60$. Although not clear in the $\bar{\omega}$ vs. $\bar{\lambda}$ plot, the frequencies of modes 2 and 3 do not really coalesce. They are so close to each other that the structure becomes unstable. Moreover, mode switching is observed between mode 4 and 5 at $\bar{\lambda} = 270.50$, as shown in the Ω_R vs. $\bar{\lambda}$ plot of Figure 3.11. Mode switching is an undesirable phenomenon that designers strive to suppress.

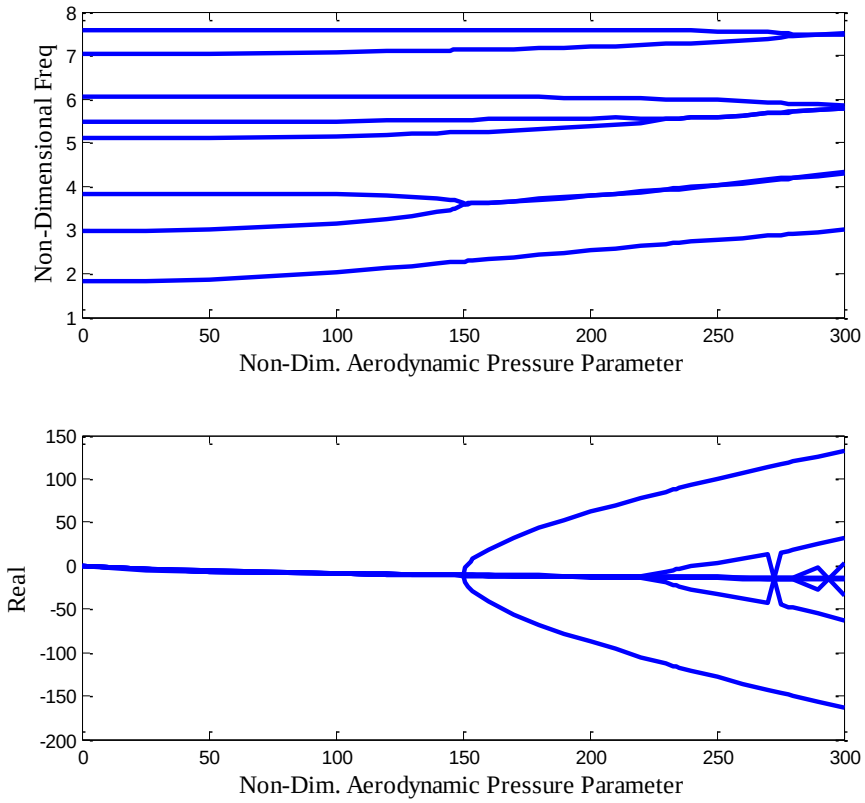

Figure 3.11 $\bar{\omega}$ vs. $\bar{\lambda}$ and Ω_R vs. $\bar{\lambda}$ for a C-C-C-C [45°/-45°/45°] laminated composite plate with one curvilinear stiffener as in Figure 3.10- b

Table 3.9 and Table 3.10 summarize the $\bar{\lambda}_{cr}$ for all case studies in Figure 3.10 with five different fiber orientations under clamped and simply supported boundary conditions, respectively. For all of the unstiffened cases, the critical coalescing mode pair is (1, 2), but adding a stiffener prevents the coalescence of mode 1 with another mode.

Table 3.9 $\bar{\lambda}_{cr}$ for different C-C-C-C laminated plate configurations

Case Study	**[0°/0°/0°]**	**[90°/90°/90°]**	**[60°/30°/60°]**	**[45°/-45°/45°]**	**[70°/60°/70°]**
Unstiffened	153.70	76.68	90.95	106.30	82.83
Figure 3.10- a	143.20	291.40	180.20	143.90	232.70
Figure 3.10- b	142.70	45.02	111.20	151.60	77.27
Figure 3.10- c	28.98	440.50	201.80	256.80	329.00
Figure 3.10- d	170.30	122.50	64.84	153.80	74.64

Table 3.10 $\bar{\lambda}_{cr}$ for different S-S-S-S laminated plate configurations

Case Study	**[0°/0°/0°]**	**[90°/90°/90°]**	**[60°/30°/60°]**	**[45°/-45°/45°]**	**[70°/60°/70°]**
Unstiffened	88.59	46.55	56.04	65.18	50.82
Figure 3.10- a	9.96	206.90	105.70	97.07	131.50
Figure 3.10- b	121.60	17.85	60.52	83.87	37.53
Figure 3.10- c	95.17	238.20	245.00	227.10	149.40
Figure 3.10- d	83.91	30.29	15.17	80.58	15.10

For the case of S-S-S-S [0°/0°/0°] laminated plates of Figure 3.10- a, and Figure 3.10- d and for the C-C-C-C [0°/0°/0°] laminated stiffened plates, except of Figure 3.10- d, the stiffeners reduce the critical pressure. Although the stiffeners increase the stiffness of the structure, they bring adjacent modes closer together, causing flutter at low speed. Also, for the [0°/0°/0°] laminated plate, adding the two curvilinear stiffeners of Figure 3.10- d does not considerably improve the $\bar{\lambda}_{cr}$. However, this is only true for this specific

stiffener configuration. For instance, for a S-S-S-S [0°/0°/0°] laminated plate with two curvilinear stiffeners oriented as shown in Figure 3.12, the $\bar{\lambda}_{cr} = 238.80$, which is larger than any other configuration presented in Table 3.10 for this laminate.

From the plot $\bar{\omega}$ vs. $\bar{\lambda}$, $\bar{\lambda}_{cr} = 235.00$ which is slightly lower than $\bar{\lambda}_{cr} = 238.80$ from the plot Ω_R vs. $\bar{\lambda}$. This is due to the fact that the aerodynamic damping removes some of the energy absorbed by the system. Therefore, the structure does not immediately experience flutter when the two modes start coalescing (Zhao & Cao, 2013).

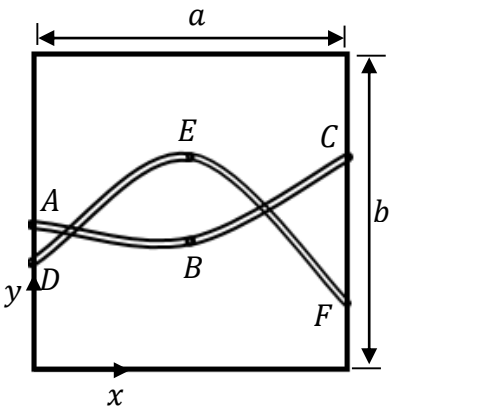

$A(0, 0.45); B(0.5, 0.3); C(1, 0.66834)$
$D(0, 0.33167); E(0.5, 0.66834); F(1, 0.33167)$

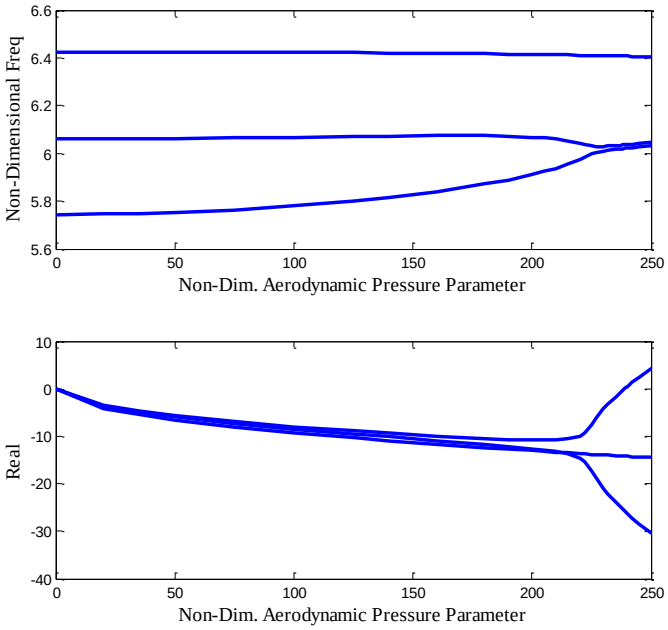

Figure 3.12 $\bar{\omega}$ vs. $\bar{\lambda}$ and Ω_R vs. $\bar{\lambda}$ for the S-S-S-S [0°/0°/0°] laminated stiffened plate on the left. Only modes 6 to 8 are illustrated since the preceding modes are not critical

The comparison of the plates with one stiffener (Figure 3.10- a and Figure 3.10- b) shows that the straight stiffener parallel to the flow is better to suppress flutter than the considered curved stiffener for all laminates, except the clamped [45°/-45°/45°] and the simply supported [0°/0°/0°]. However, this is only true for this specific curvilinear stiffener

(Figure 3.10-b) as will be discussed later. In addition, increasing the number of curvilinear stiffeners does not guarantee a better flutter performance than a single stiffener. For all cases, except the C-C-C-C [0°/0°/0°] laminated plate of Figure 3.10-d, two straight stiffeners yield a higher $\bar{\lambda}_{cr}$ than two curvilinear stiffeners. As can be seen, there is a correlation between the fiber orientation and the number and shape of the stiffeners. Therefore, we cannot study the effect of these variables individually. Both fiber and stiffener orientation variables should be considered in the design process and cannot be implemented at different levels during optimization.

To further demonstrate the effect of the stiffener and fiber orientation on the flutter speed, several mutations of the stiffener in Figure 3.10-b are considered in Table 3.11 and Table 3.12. In the cases studied here, the middle coordinate (point B) of the stiffener is varied, increasing the $\bar{\lambda}_{cr}$ (for all of the cases, except the [0°/0°/0°] and [45°/45°/45°] laminated plate) as point B moved closer to the center. In the last case of Table 3.11 and Table 3.12, point A is moved instead of point B, and very optimistic results are achieved for most of the fiber orientations, implying that many other configurations can be considered. The best stiffener's configuration for each laminate are marked in bold. The results in Table 3.11 and Table 3.12 prove that the stiffener's shape combined with the fiber orientation can be used for the passive control of the flutter speed.

Table 3.11 $\bar{\lambda}_{cr}$ of C-C-C-C plates with a single curvilinear stiffener

Configurations	[0°/0°/0°]	[90°/90°/90°]	[60°/30°/60°]	[45°/-45°/45°]	[70°/60°/70°]
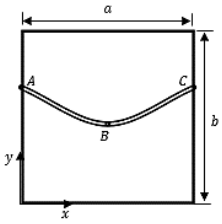	11.67	**197.80**	177.90	145.30	**195.10**
	(3,4)	(2, 3)	(6, 7)	(3, 4)	(6, 7)
$A(0,0.66834); B(0.5,0.45); C(1,0.66834)$					
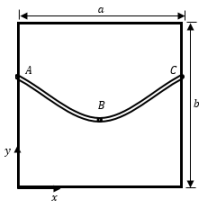	58.00	101.00	177.70	207.50	134.40
	(7, 8)	(2, 3)	(2, 3)	(8, 9)	(2, 3)
$A(0,0.66834); B(0.5,0.4); C(1,0.66834)$					
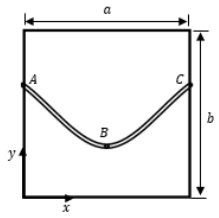	51.77	28.71	94.62	134.40	61.75
	(12, 13)	(2, 3)	(2, 3)	(2, 3)	(2, 3)
$A(0,0.66834); B(0.5,0.3); C(1,0.66834)$					
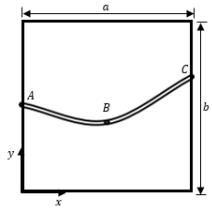	**249.70**	126.30	**210.80**	**236.10**	169.20
	(2, 3)	(2, 3)	(2, 3)	(2, 3)	(2, 3)
$A(0,0.5); B(0.5,0.4); C(1,0.66834)$					

Table 3.12 $\bar{\lambda}_{cr}$ of S-S-S-S plates with a single curvilinear stiffener

Configurations	[0°/0°/0°]	[90°/90°/90°]	[60°/30°/60°]	[45°/-45°/45°]	[70°/60°/70°]
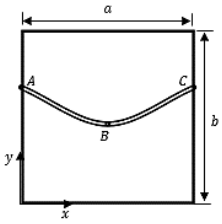	10.07	**95.81**	**166.10**	120.90	**134.05**
	(3, 4)	(2, 3)	(7, 8)	(4, 5)	(2, 3)
$A(0,0.66834); B(0.5,0.45); C(1,0.66834)$					
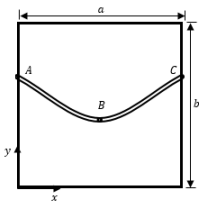	21.25	46.90	104.30	136.20	70.95
	(3, 4)	(2, 3)	(2, 3)	(2, 3)	(2, 3)
$A(0,0.66834); B(0.5,0.4); C(1,0.66834)$					
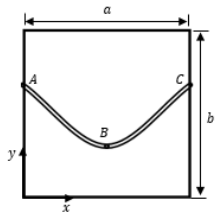	**110.00**	9.73	50.13	72.47	29.30
	(2, 3)	(2, 3)	(2, 3)	(2, 3)	(2, 3)
$A(0,0.66834); B(0.5,0.3); C(1,0.66834)$					
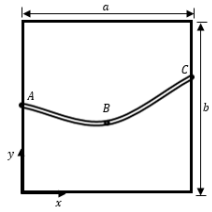	99.58	66.29	78.53	**157.01**	97.56
	(3. 4)	(2, 3)	(2, 3)	(2, 3)	(2, 3)
$A(0,0.5); B(0.5,0.4); C(1,0.66834)$					

Table 3.11 and Table 3.12 illustrate that choosing the right shape for the stiffener with respect to the laminate properties can sometimes lead to $\bar{\lambda}_{cr}$ greater than those for plates with multiple stiffeners. For the all-edge clamped plates (Table 3.11), the best configuration is the last [45°/45°/45°] laminated plate of Table 3.11. For the all-edge simply supported plates (Table 3.12), the best configuration is achieved with the first [60°/30°/60°] laminated stiffened plate of Table 3.12. Furthermore, Table 3.11 and Table 3.12 show that the coalescing modes change not only with the fiber orientation but also with the stiffener's configuration. For some of the cases, e.g. the [90°/90°/90°] laminated plates in Table 3.11, the first coalescing modes is (2, 3); for other cases, e.g. the first [0°/0°/0°], [45°/-45°/45°] and [90°/90°/90°] laminated stiffened plates in Table 3.12, the first coalescing modes are (3, 4), (4, 5), (7, 8), respectively. These findings substantiate the idea that the shape of the stiffener can be used to eliminate some flutter modes as will be further explored next.

The all-edge clamped unstiffened [45°/-45°/45°] laminated plate from Table 3.9 is reconsidered, and its mode shapes are illustrated in Table 3.13. Table 3.13 shows that as the aerodynamic pressure increases, modes 1 and 2 start approaching each other and coalesce at the critical dynamic pressure. However, flutter only occurs later because damping dissipates part of the energy absorbed by the structure.

Table 3.13 Mode shapes for a C-C-C-C unstiffened [45°/-45°/45°] laminated plate

Natural Mode Shapes	**Mode Shapes, $\lambda = 90$**	**Flutter Mode Shapes**
Mode 1, $\omega = 38.53$ Hz	Mode 1, $\omega = 57.47$ Hz	Mode (1, 2), $\lambda = 106.30$
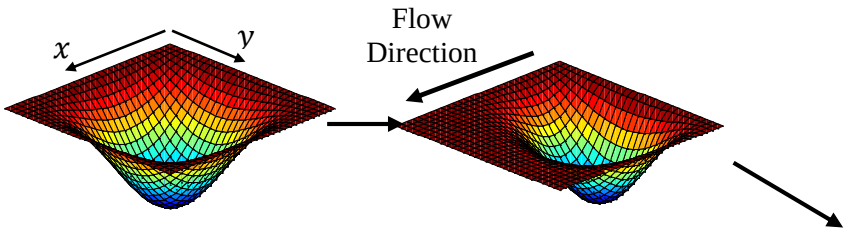		
Mode 2, $\omega = 74.25$ Hz	Mode 2, $\omega = 74.57$ Hz	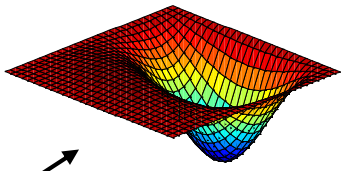
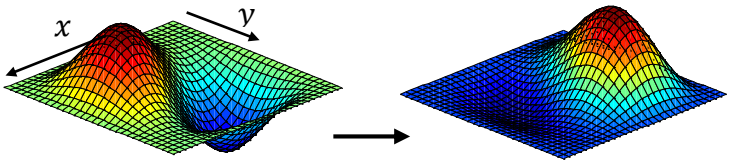		
Mode 3, $\omega = 82.11$ Hz	Mode 3, $\omega = 85.66$ Hz	Mode (3, 4), $\lambda = 210.00$
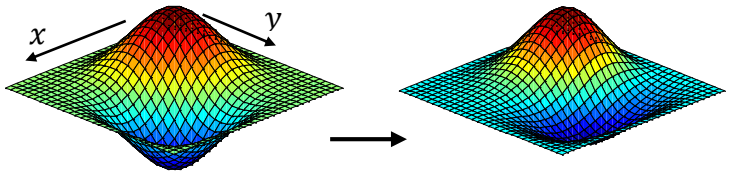		
Mode 4, $\omega = 113.59$ Hz	Mode 4, $\omega = 114.51$ Hz	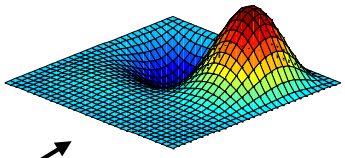
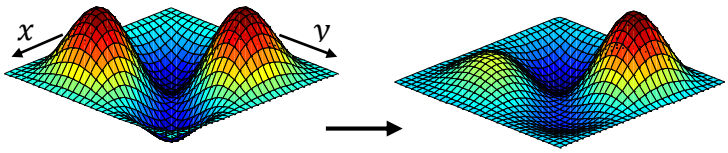		

For the unstiffened plate, increasing the dynamic pressure causes the frequencies of modes 1 and 2 to approach each other and coalesce at $\lambda = 105.00$. The system is stable, and modes 1 and 2 exhibit the same negative damping. As the dynamic speed continues to increase beyond $\lambda = 105.00$, the damping of mode 1 increases and becomes positive at $\lambda = 106.30$, whereas the damping of mode 2 decreases. At $\lambda = 106.30$, the structure becomes unstable and flutter occurs. Around $\lambda = 335.30$, the damping of mode 1 becomes negative again and of mode 2 becomes positive. The frequencies of both modes switch. Similar behavior can be perceived for some of the other modes. The described phenomenon can be observed in Table 3.14.

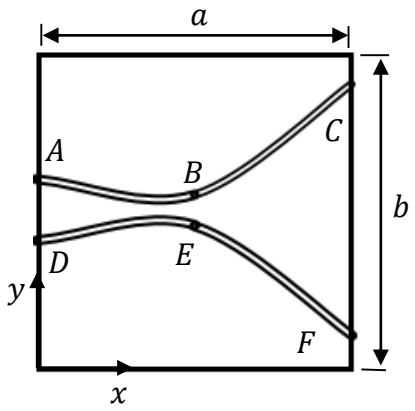

$A(0, 0.6); B(0.5, 0.55); C(1, 0.9)$
$D(0, 0.4); E(0.5, 0.45); F(1, 0.1)$

Figure 3.13 Square plate with two curvilinear stiffeners

Next, two curvilinear stiffeners are considered as an attempt to eliminate low frequency flutter modes of the [45°/-45°/45°] laminated plate under discussion. This can be achieved by observing the flutter modes of the unstiffened plate (Table 3.13) and choosing the stiffeners' path perpendicular to the deflection contour of the panel and that runs through as many points of large deflection in lower modes as possible. The stiffeners'

configuration chosen is shown in Figure 3.13.

In general, the curvilinear stiffeners prevent the coalescence of lower modes. In this case, placing two curvilinear stiffeners in the plate prevents modes 1 and 2 from coalescing and substantially increases the modal frequencies, the critical frequency and the critical dynamic pressure.

Table 3.14 $\bar{\omega}$ vs. $\bar{\lambda}$ and α vs. $\bar{\lambda}$ for the C-C-C-C [45°/-45°/45°] laminated unstiffened and stiffened plate

Unstiffened Plate	**Curvilinear-Stiffened Plate**
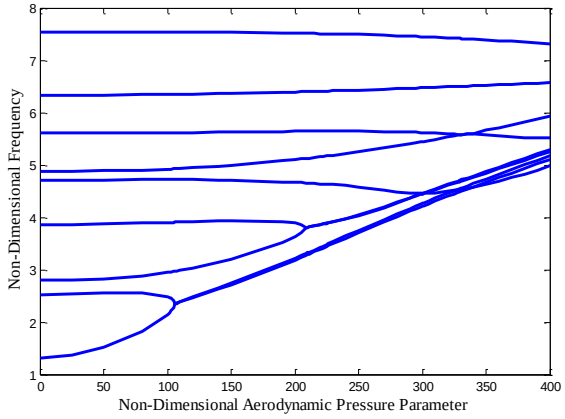	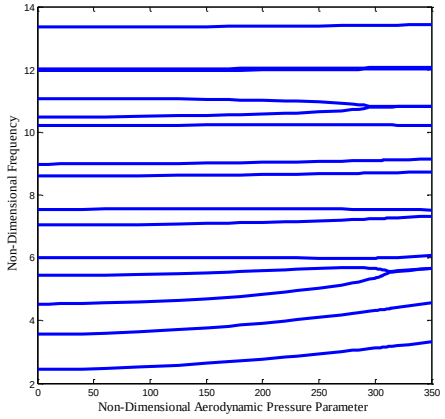
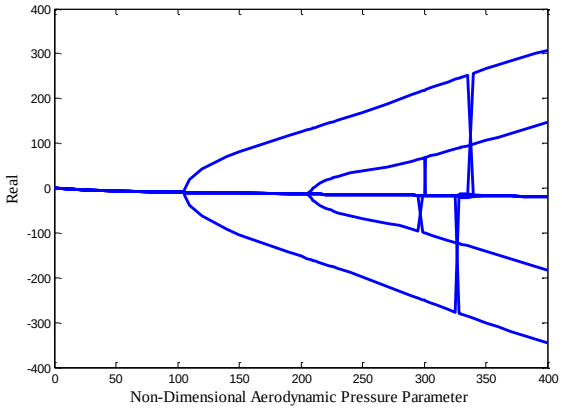	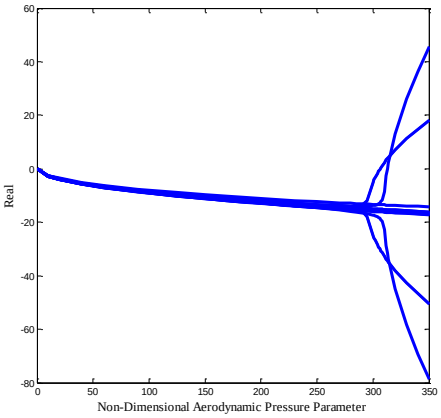

Table 3.15 Mode shapes for C-C-C-C [45°/-45°/45°] laminated plate with two curvilinear stiffeners

Natural Mode Shapes	**Mode Shapes, $\lambda = 240$**	**Flutter Mode Shapes**
Mode 1, $\omega = 70.87$ Hz	Mode 1, $\omega = 85.41$ Hz	
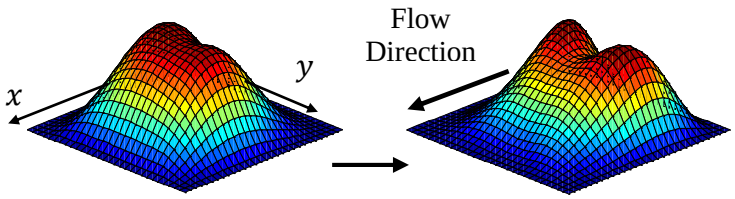		
Mode 2, $\omega = 109.19$ Hz	Mode 2, $\omega = 119.49$ Hz	
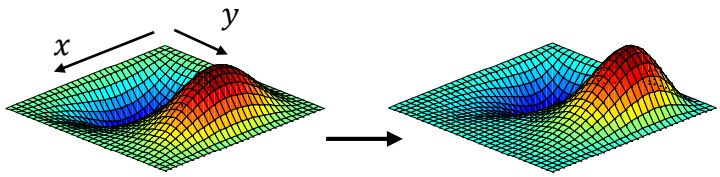		
Mode 3, $\omega = 132.25$ Hz	Mode 3, $\omega = 146.60$ Hz	Mode (3, 4), $\lambda = 312.70$
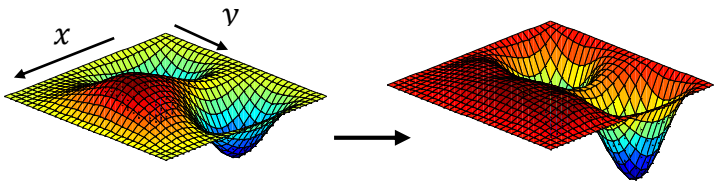		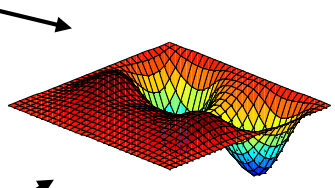
Mode 4, $\omega = 163.37$ Hz	Mode 4, $\omega = 165.89$ Hz	
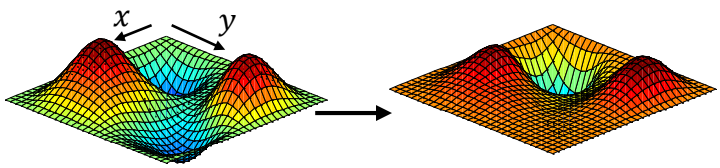		

Natural Mode Shapes	Mode Shapes, $\lambda = 240$	Flutter Mode Shapes
Mode 11, $\omega = 310.96$ Hz	Mode 11, $\omega = 312.42$ Hz	Mode (11, 12), $\lambda = 306.90$
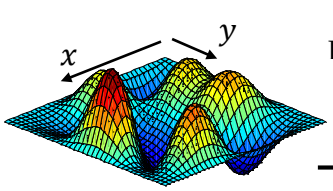	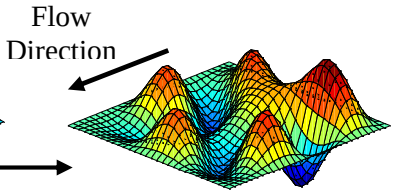	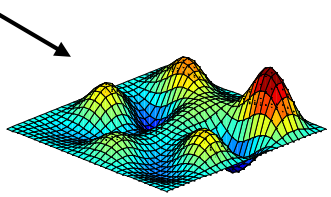
Mode 12, $\omega = 325.59$ Hz	Mode 12, $\omega = 322.49$ Hz	
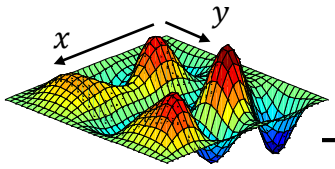	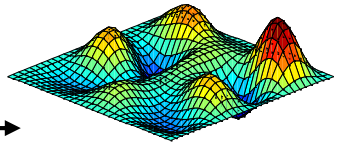	

As can be seen in Table 3.15, for the stiffened plate, the critical coalescing pair of modes is no longer 1 and 2. It is instead modes 11 and 12, and the $\bar{\lambda}_{\mathrm{cr}} = 306.90$. These observations substantiate the theory that curvilinear stiffeners can eliminate some of the flutter mode shapes and hence, prevent flutter.

3.2.4. Flutter of Skew Plates

The effectiveness of curvilinear stiffeners in the flutter prevention of laminated skew plates is studied. Unstiffened and curvilinear-stiffened plates with 0°, 15° and 30° skew angle are considered. The same stiffener configuration represented in Figure 3.13 is considered. For laminates here considered, clamped or simply supported on all edges, the $\bar{\lambda}_{cr}$ increases as the skew angle increases, independently from the fiber orientation. The

explanation for this phenomenon is that increasing the skew angle causes an increase in the natural frequencies and in the difference between adjacent modal frequencies. Additionally, for all skew angles, the $\bar{\lambda}_{cr}$ decreases as the ply angle increases from 0° to 90°. These remarks can be observed in Table 3.16 and Table 3.17 and are consistent with Chowdary, Sinha and Parthan (1996) and Koo and Hwang (2004).

Contrary to unstiffened plates, the relation between the $\bar{\lambda}_{cr}$ and the skew angle of stiffened plates depends on the fiber angle and boundary conditions. For the all-edge clamped [60°/30°/60°] laminates, the $\bar{\lambda}_{cr}$ increases as the skew angle increases. For all of the other clamped cases in Table 3.19, the $\bar{\lambda}_{cr}$ for the 15° skew angle is smaller than for the 0° and 30° skew angle. The clamped and simply supported [45°/-45°/45°] laminated 15° skew plates have similar $\bar{\lambda}_{cr}$. Further analysis shows that these remarks are only true for the considered stiffener configuration. The described behavior is depicted in Table 3.18 and Table 3.19.

Table 3.16 $\bar{\lambda}_{cr}$ of C-C-C-C skew unstiffened plates

Skew Angle	**[0°/0°/0°]**	**[90°/90°/90°]**	**[60°/30°/60°]**	**[45°/-45°/45°]**	**[70°/60°/70°]**
0°	153.70	76.68	90.95	106.30	82.83
15°	155.10	82.96	101.04	115.70	91.26
30°	168.81	105.40	126.90	141.50	117.20

Table 3.17 $\bar{\lambda}_{cr}$ of S-S-S-S skew unstiffened plates

Skew Angle	**[0°/0°/0°]**	**[90°/90°/90°]**	**[60°/30°/60°]**	**[45°/-45°/45°]**	**[70°/60°/70°]**
0°	88.59	46.55	56.04	65.18	50.82
15°	89.25	50.17	60.84	68.55	55.17
30°	97.88	60.19	73.83	82.38	68.81

In addition, the flutter coalescing modes for the unstiffened cases in Table 3.16 and Table 3.17 are modes (1, 2), whereas for the curvilinear-stiffened plates, they are in most cases high modes. This implies that the curvilinear stiffener suppressed the coalescence of lower modes. Comparing Table 3.16 through Table 3.19 leads to the conclusion that there is also a correlation between the skew angle and stiffener and fiber orientation, and they cannot be individually designed.

Table 3.18 $\bar{\lambda}_{cr}$ of C-C-C-C laminated skew plates with two curvilinear stiffeners

Skew Angle	**[0°/0°/0°]**	**[90°/90°/90°]**	**[60°/30°/60°]**	**[45°/-45°/45°]**	**[70°/60°/70°]**
0°	343.60 (3, 4)	225.00 (15, 16)	211.70 (16, 17)	306.90 (11, 12)	182.50 (16, 17)

15°	164.80	150.35	218.70	190.30	70.17
	(3, 4)	(5, 6)	(5, 6)	(6, 7)	(5, 6)
30°	410.10	225.90	275.20	346.30	204.60
	(17, 18)	(10, 11)	(7, 8)	(7, 8)	(7, 8)

Table 3.19 $\bar{\lambda}_{cr}$ of S-S-S-S skew plates with two curvilinear stiffeners

Skew Angle	**[0°/0°/0°]**	**[90°/90°/90°]**	**[60°/30°/60°]**	**[45°/-45°/45°]**	**[70°/60°/70°]**
0°	62.87	303.90	174.70	167.80	230.20
	(11, 12)	(16,17)	(3, 4)	(3, 4)	(3, 4)
15°	130.50	66.39	77.68	196.70	46.88
	(3, 4)	(5, 6)	(6, 7)	(6, 7)	(6, 7)
30°	359.90	248.10	223.90	250.90	215.90
	(2, 3)	(7, 8)	(7, 8)	(5, 6)	(7, 8)

Table 3.20 shows the plots of $\bar{\omega}$ vs. $\bar{\lambda}$ and Ω_R vs. $\bar{\lambda}$ for the unstiffened and curvilinear-stiffened C-C-C-C 30° skew plates. By introducing two curvilinear stiffeners, the critical coalescing modes shift from modes (1, 2) to modes (7, 8), and the modal

frequencies and $\bar{\lambda}_{cr}$ increase. For the considered unstiffened plate, the natural frequencies of modes 3 and 4 are very close to each other, and they appear as a single mode in Table 3.20, but they are distinct.

Table 3.20 $\bar{\omega}$ vs. $\bar{\lambda}$ and Ω_R vs. $\bar{\lambda}$ plots for the C-C-C-C [45°/-45°/45°] laminated 30° skew plates

Unstiffened Plate	**Curvilinear-Stiffened Plate**
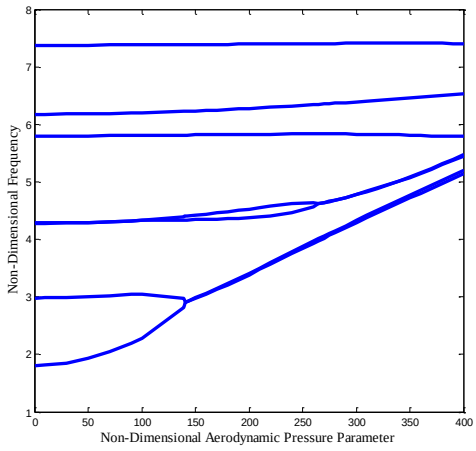	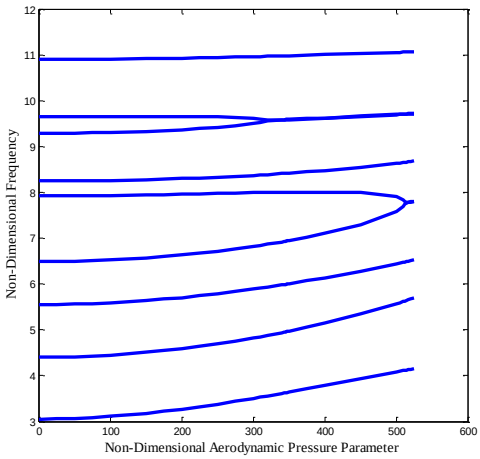
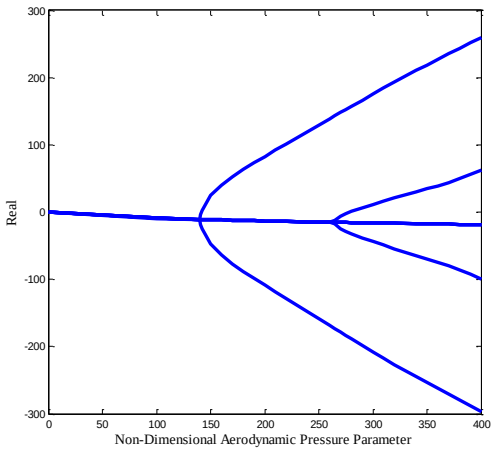	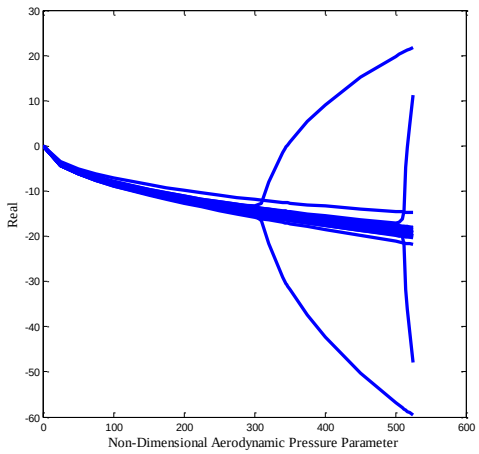

Table 3.21 First four mode shapes for C-C-C-C [45°/-45°/45°] laminated 30° skew plate with no stiffeners

Natural Mode Shapes	**Mode Shapes, $\lambda = 90$**	**Flutter Mode Shapes**
Mode 1, $\omega = 53.12$ Hz	Mode 1, $\omega = 64.45$ Hz	Mode (1, 2), $\lambda = 141.50$
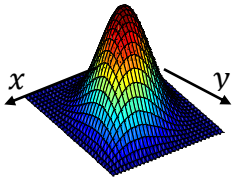	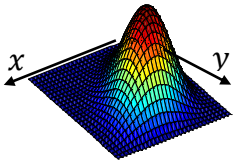	
Mode 2, $\omega = 87.63$ Hz	Mode 2, $\omega = 89.46$ Hz	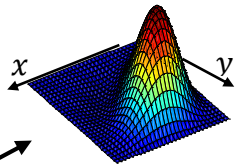
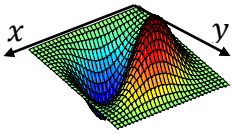	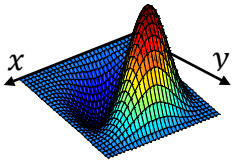	
Mode 3, $\omega = 125.70$ Hz	Mode 3, $\omega = 126.95$ Hz	Mode (3, 4), $\lambda = 278.80$
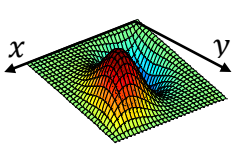	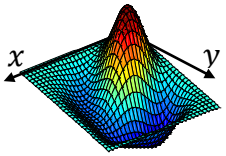	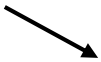
Mode 4, $\omega = 126.08$ Hz	Mode 4, $\omega = 126.96$ Hz	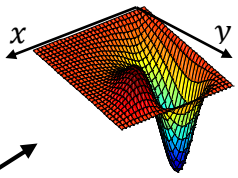
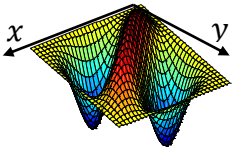	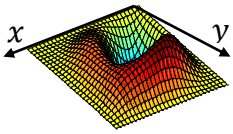	

Table 3.22 Mode shapes for C-C-C-C [45°/-45°/45°] laminated 30° skew plate with two curvilinear stiffeners

Natural Mode Shapes	**Mode Shapes, $\lambda = 280$**	**Flutter Mode Shapes**
Mode 4, $\omega = 182.49$ Hz	Mode 4, $\omega = 199.15$ Hz	Mode (4, 5), $\lambda = 517.20$
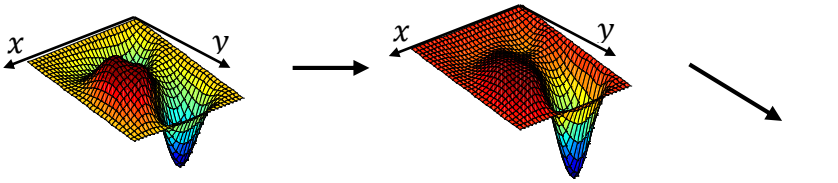		
Mode 5, $\omega = 229.55$ Hz	Mode 5, $\omega = 234.68$ Hz	
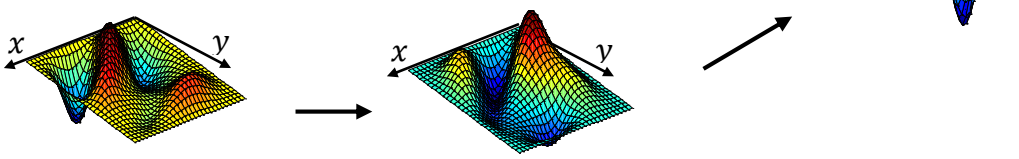		
Mode 7, $\omega = 265.23$ Hz	Mode 7, $\omega = 278.13$ Hz	Mode (7, 8), $\lambda = 346.30$
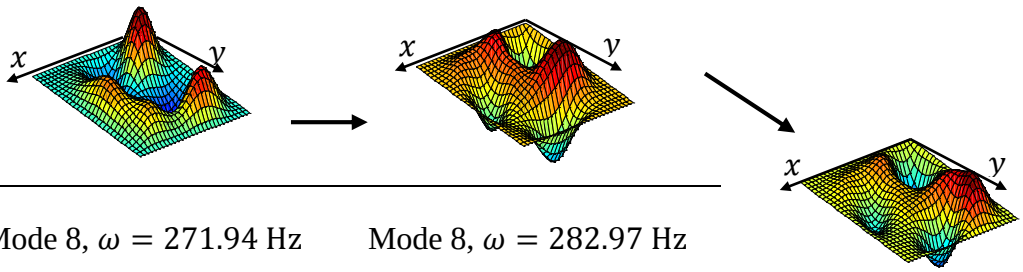		
Mode 8, $\omega = 271.94$ Hz	Mode 8, $\omega = 282.97$ Hz	
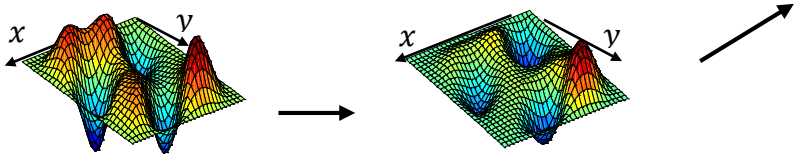		

Table 3.21 and Table 3.22 illustrate the mode shapes for the unstiffened and

stiffened skew plates in study. The shapes demonstrate that for the stiffened plate, flutter occurs at higher frequencies because the stiffeners cause higher adjacent modes to become closer to each other. Table 3.16 through Table 3.22 clearly demonstrate that the stiffener's shape and fiber orientation can be utilized to tailor the flutter behavior of the skew panels.

3.3. Free Vibration of Wing Boxes

Four wing models with uniform thicknesses are now considered to attest the accuracy of the proposed methodology. The skin, spars and ribs are modeled using SHELL181 in ANSYS®. The [45°/-45°/45°] laminated wing models considered in this section are clamped at the root (at $x = 0$) and made of T300/5208 graphite/epoxy composite with the following mechanical properties: $E_1 = 132.38\ GPa$, $E_2 = 10.7\ GPa$, $G_{12} = G_{13} = 5.65\ GPa$, $G_{23} = 3.38\ GPa$, $\nu_{12} = \nu_{13} = 0.24$, $\nu_{23} = 0.49$ and $\rho = 1800\ \frac{kg}{m^3}$ (Zhao & Kapania, 2016).

3.3.1. Vibration of Rectangular Wing Boxes

Although in practice more complex designs are common, a rectangular composite wing box is now considered for simplicity. The box with four spars and six ribs has a semi-span of 4.29 m, a chord of 0.849 m and a thickness of 42.45 mm. The top and bottom skins are 3.0 mm, and the spars and ribs are 1.5 mm thick.

Table 3.23 gives the natural frequencies and corresponding mode shapes for the wing box with straight spars and ribs as represented in Figure 3.14. The coordinates of the spars and ribs for this wing are listed in Table 3.24 where point 1, 2 and 3 represent the initial, middle and final points of the spar or ribs, respectively. The results in Table 3.23

are in good agreement with those obtained from ANSYS®.

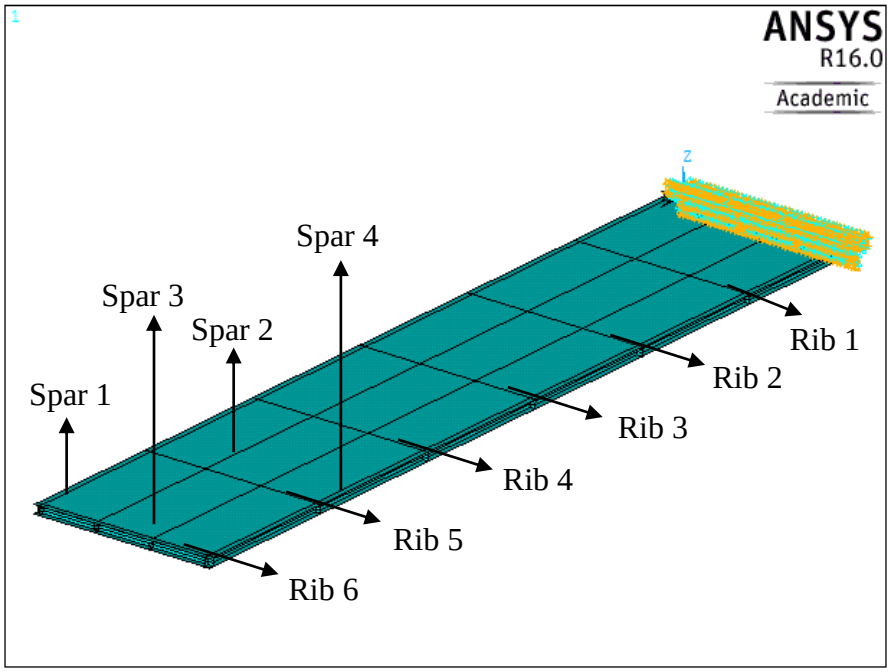

Figure 3.14 Wing box with four spars and six ribs

Table 3.23 First five modes of vibration of a wing box with four straight spars and six straight ribs

Present	**ANSYS®**	**% Error**
Mode 1, $\omega = 2.16$	Mode 1, $\omega = 2.05$	5.37
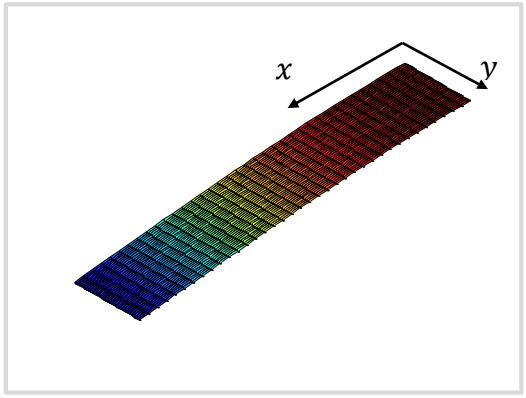	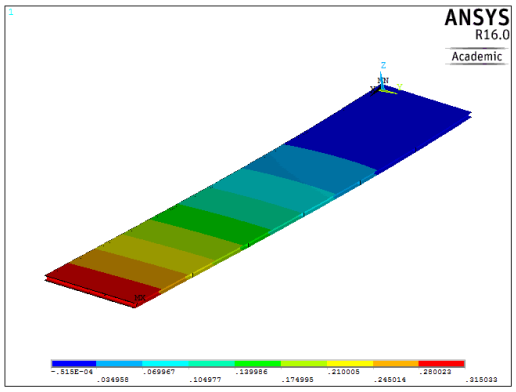	

Present	ANSYS®	% Error
Mode 2, $\omega = 13.50$	Mode 2, $\omega = 12.75$	5.88
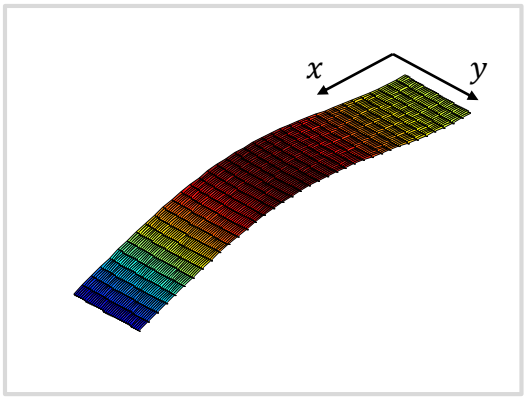	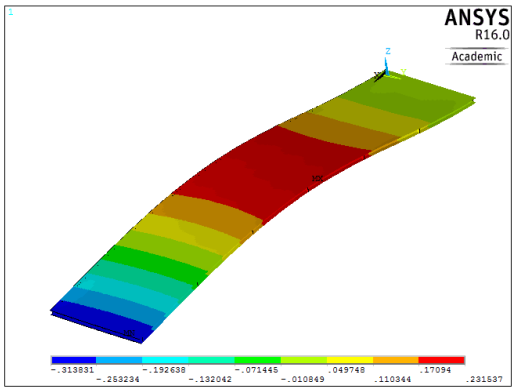	
Mode 3, $\omega = 36.65$	Mode 3, $\omega = 32.95$	10.96
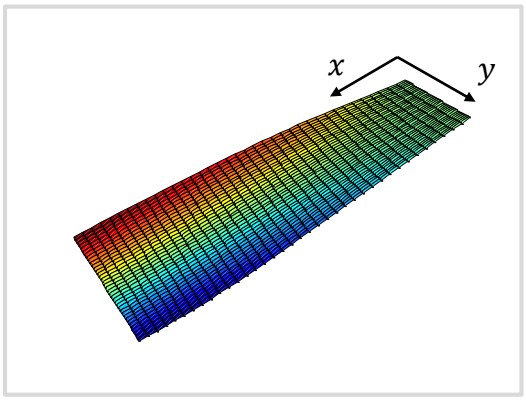	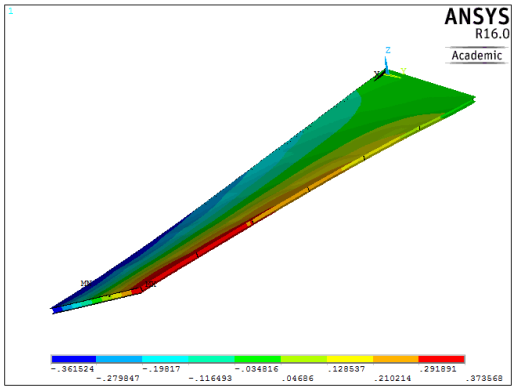	
Mode 4, $\omega = 38.66$	Mode 4, $\omega = 35.56$	8.72
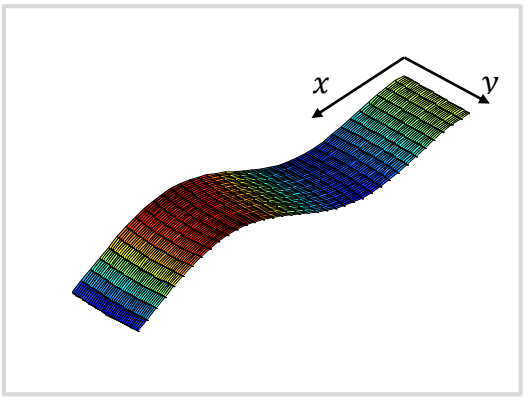	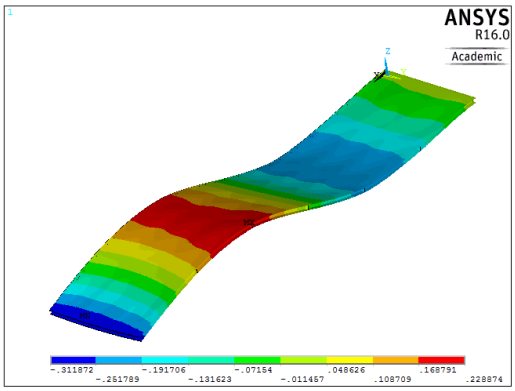	

Present	ANSYS®	% Error
Mode 5, $\omega = 77.70$	Mode 5, $\omega = 67.81$	14.58
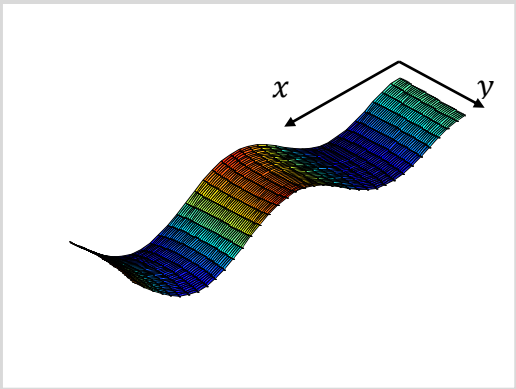	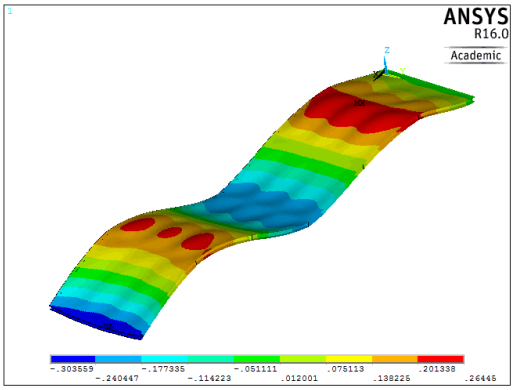	

Table 3.24 Coordinates of three points of the spars and ribs in Figure 3.14

Spar or Rib	Point	X (mm)	Y (mm)	Spar or Rib	Point	X (mm)	Y (mm)
	1	0	25		1	1422	0
Spar 1	2	2145	25	Rib 2	2	1422	425
	3	4290	25		3	1422	849
	1	0	292		1	2132	0
Spar 2	2	2145	292	Rib 3	2	2132	425
	3	4290	292		3	2132	849
	1	0	824		1	2843	0
Spar 3	2	2145	824	Rib 4	2	2843	425
	3	4290	824		3	2843	849

	1	0	558		1	3554	0
Spar 4	2	2145	558	Rib 5	2	3554	425
	3	4290	558		3	3554	849
	1	711	0		1	4265	0
Rib 1	2	711	425	Rib 6	2	4265	425
	3	711	849		3	4265	849

The curvature of the spars and ribs of the wing box in discussion are modified as shown in Figure 3.15. The coordinates of the spars and ribs for the modified wing are listed in Table 3.26. The mode shapes and natural frequencies are given by Table 3.25. A reasonable agreement is obtained between the present study and ANSYS® for all modes except the torsional mode (mode 3). The existing discrepancy might be due to the fact that the present study neglects the rotation about the *z* axis which is considered in ANSYS®.

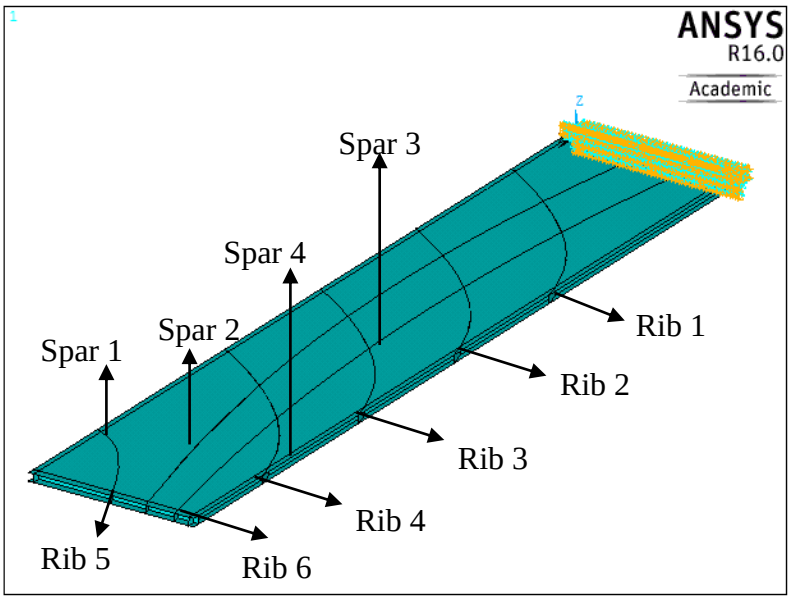

Figure 3.15 Wing box with curvilinear spars and ribs

Table 3.25 First four modes of vibration of a wing box with four curvilinear spars and six curvilinear ribs

Present	**ANSYS®**	**% Error**
Mode 1, $\omega = 2.24$	Mode 1, $\omega = 2.29$	2.18
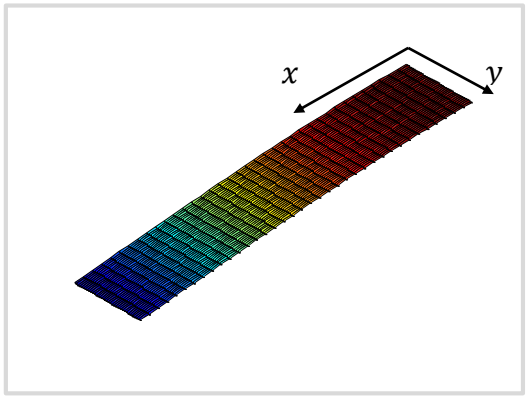	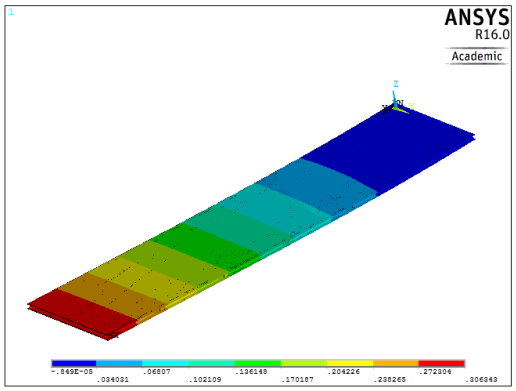	
Mode 2, $\omega = 13.57$	Mode 2, $\omega = 14.55$	6.74
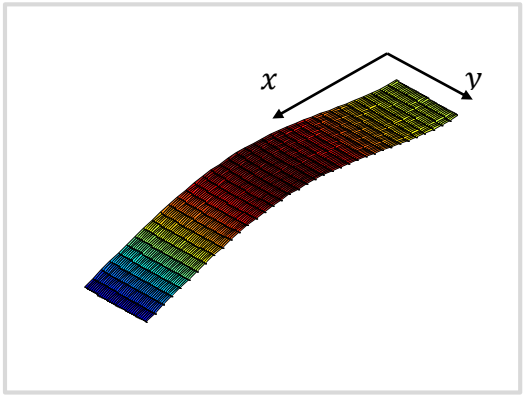	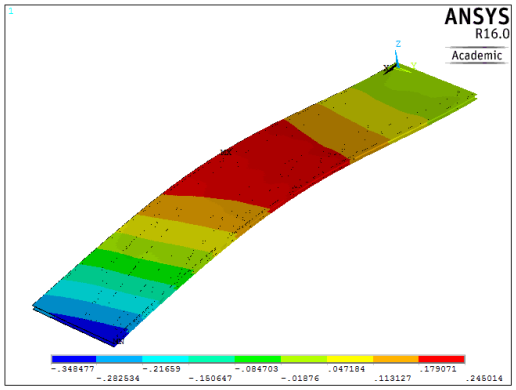	
Mode 3, $\omega = 36.44$	Mode 3, $\omega = 26.19$	39.14

Present	ANSYS®	% Error
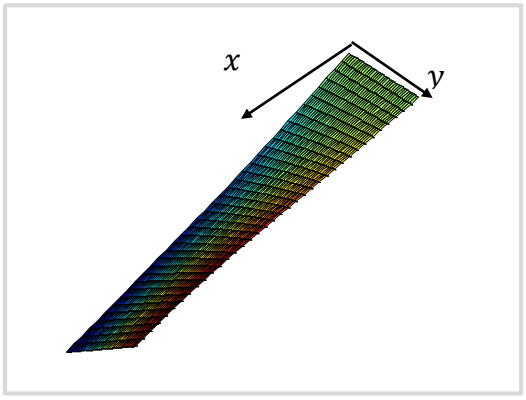	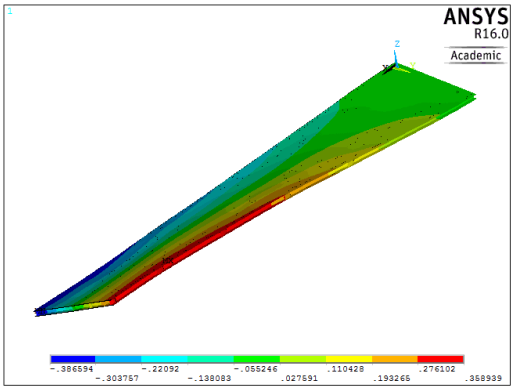	
Mode 4, $\omega = 38.59$	Mode 4, $\omega = 40.35$	4.36
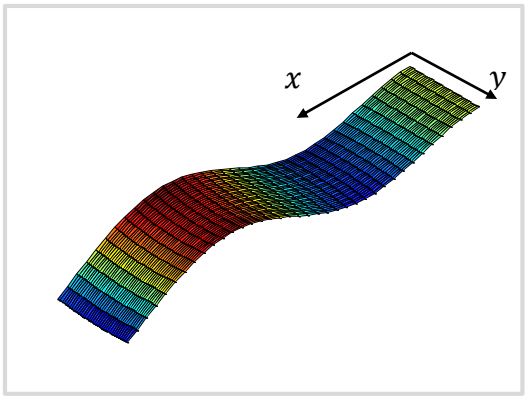	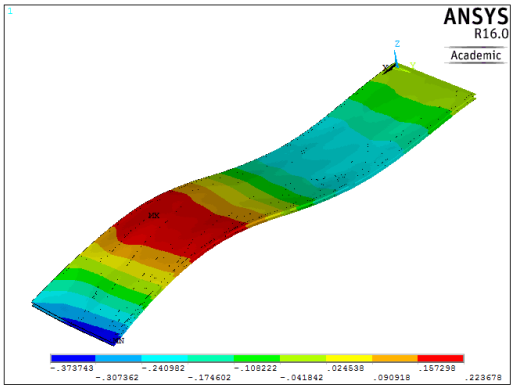	

Table 3.26 Coordinates of three points of the spars and ribs in Figure 3.15

Spar or Rib	Point	X (mm)	Y (mm)	Spar or Rib	Point	X (mm)	Y (mm)
	1	0	25		1	1250	0
Spar 1	2	2145	25	Rib 2	2	1750	600
	3	4290	25		3	2250	849

Spar or Rib	Point	X (mm)	Y (mm)	Spar or Rib	Point	X (mm)	Y (mm)
	1	0	400		1	2000	0
Spar 2	2	2145	250	Rib 3	2	2500	600
	3	4290	600		3	3000	849
	1	0	650		1	2750	0
Spar 3	2	2145	500	Rib 4	2	3250	600
	3	4290	750		3	3750	849
	1	0	824		1	3750	0
Spar 4	2	2145	824	Rib 5	2	3900	600
	3	4290	824		3	4290	849
	1	500	0		1	4250	0
Rib 1	2	1000	600	Rib 6	2	4250	425
	3	1500	849		3	4250	849

Comparing Table 3.23 to Table 3.25, one can observe that the curvilinear spars and ribs have no significant impact on the vibration of the wing box when compared to their straight counterpart. A more detailed study is necessary to evaluate the effects of the internal structures' shape on the response of a wing. Also, optimization studies should be considered in order to find an optimal path for the spars and ribs under some constraints. However, all of these aspects are beyond the scope of this research.

3.3.2. Vibration of a Swept Wing Box

The model in this section is a 30° swept wing with constant chord and four spars and six ribs. The wing has a semi-span of 3.715 m, a chord of 0.849 m and a thickness of 42.45 mm. The top and bottom skins are 3.0 mm, and the spars and ribs are 1.5 mm thick. The wing with four curvilinear spars and six ribs is represented in Figure 3.16, and the coordinates of its internal structures are listed in Table 3.28.

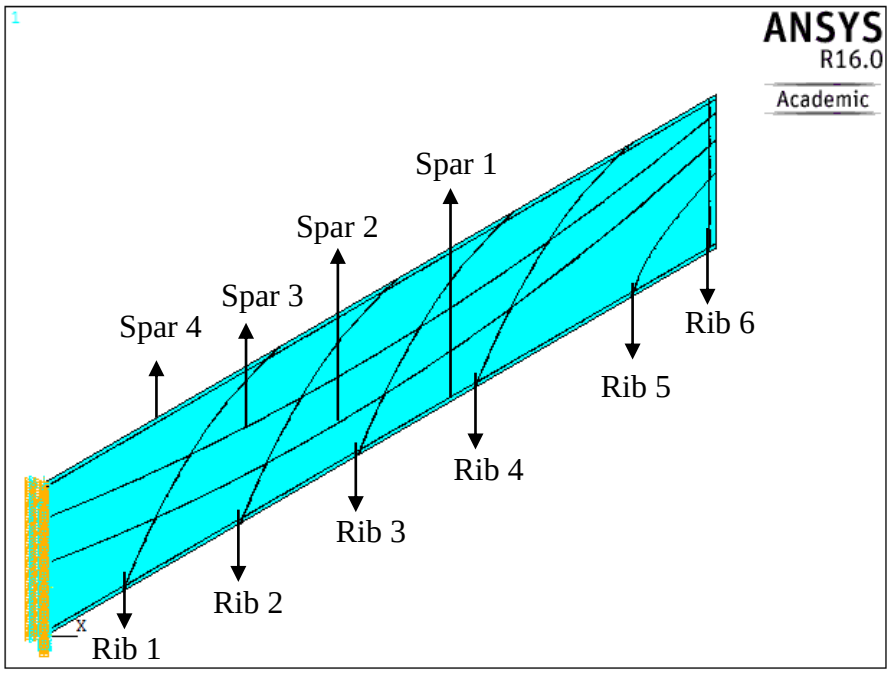

Figure 3.16 Top view of a 30° sweptback wing with curvilinear spars and ribs

The mode shapes and natural frequencies for the referred wing correlate well with the ANSYS® model as shown in Table 3.27. The existing error is due to the same reason pointed out for the previous wing model.

Table 3.27 First four modes of vibration of a swept wing box with curvilinear spars and ribs

Present	ANSYS®	% Error
Mode 1, $\omega = 2.68$	Mode 1, $\omega = 2.50$	7.20
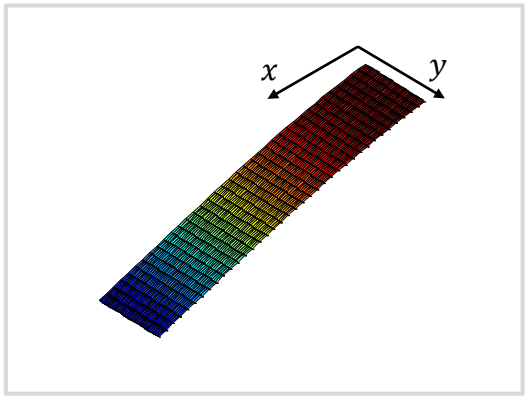	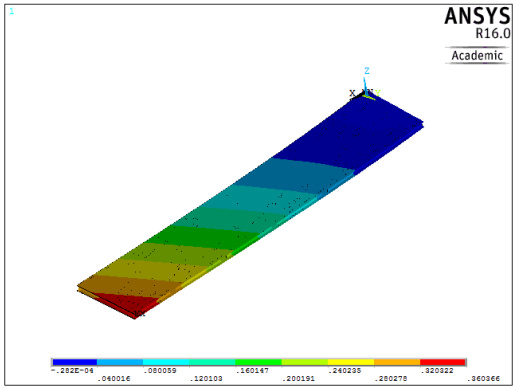	
Mode 2, $\omega = 16.65$	Mode 2, $\omega = 14.42$	15.46
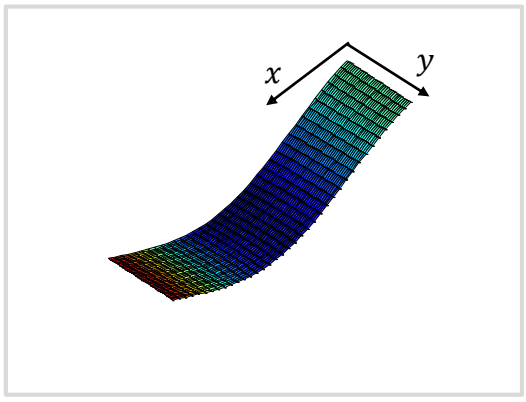	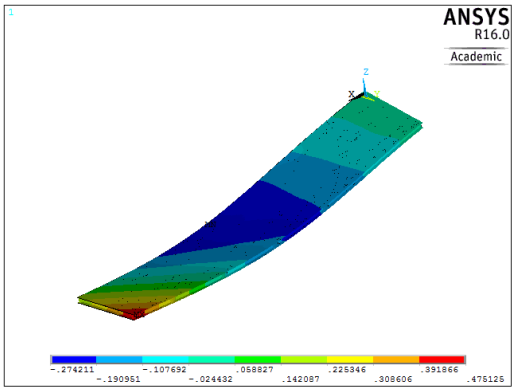	
Mode 3, $\omega = 24.42$	Mode 3, $\omega = 30.89$	20.95

Present	ANSYS®	% Error
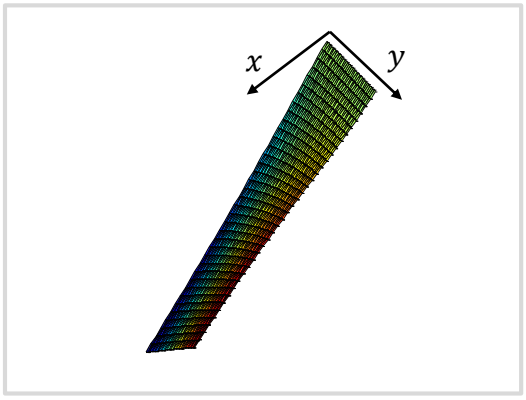	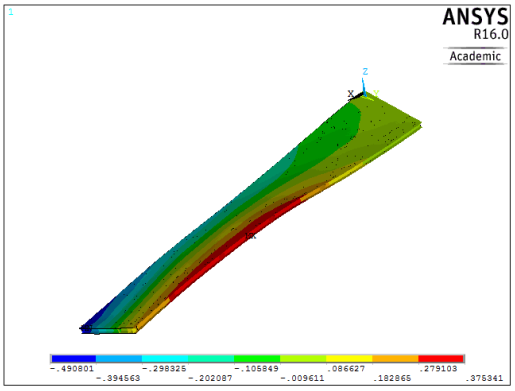	
Mode 4, $\omega = 46.55$	Mode 4, $\omega = 41.02$	13.48
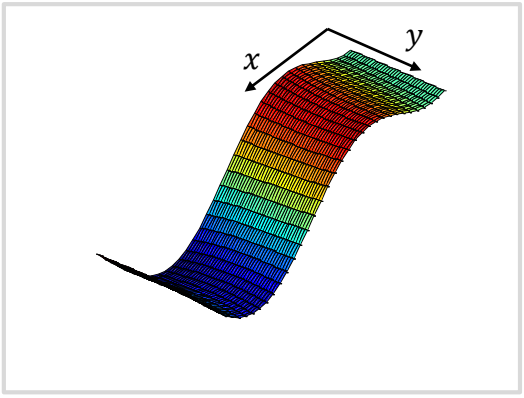	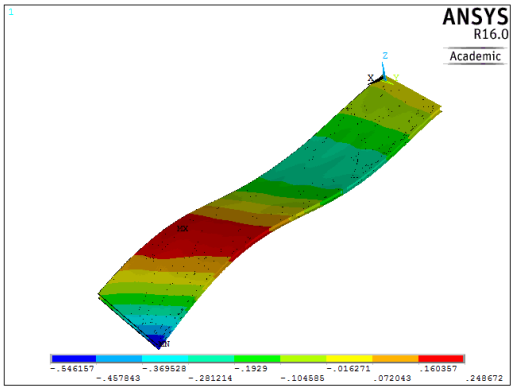	

Table 3.28 Coordinates of three points of the spars and ribs in Figure 3.16

Spar or Rib	Point	X (mm)	Y (mm)	Spar or Rib	Point	X (mm)	Y (mm)
	1	0	25		1	1083	625
Spar 1	2	1858	1097	Rib 2	2	1516	1475
	3	3715	2170		3	1949	1974

Spar or Rib	Point	X (mm)	Y (mm)	Spar or Rib	Point	X (mm)	Y (mm)
	1	0	400		1	1732	1000
Spar 2	2	1858	1323	Rib 3	2	2165	1850
	3	3715	2745		3	2598	2724
	1	0	650		1	2382	1375
Spar 3	2	1858	1573	Rib 4	2	2815	2225
	3	3715	2895		3	3248	2724
	1	0	824		1	3248	1875
Spar 4	2	1858	1896	Rib 5	2	3377	2150
	3	3715	2969		3	3715	2565
	1	433	250		1	3681	2125
Rib 1	2	866	1100	Rib 6	2	3681	2550
	3	1299	1599		3	3681	2974

3.3.3. Vibration of a Tapered Wing Box

The last case considered is a wing with tapered trailing edge (T.E.) as shown in Figure 3.17. The wing has a semi-span of 4.293 m, a root chord of 1.626 m, a tapered ratio of 0.67 and a thickness of 54.55 mm. The top and bottom skins are 3.0 mm, and the spars and ribs are 1.5 mm thick. This wing has four curvilinear spars and ten curvilinear ribs whose coordinates are listed in Table 3.29.

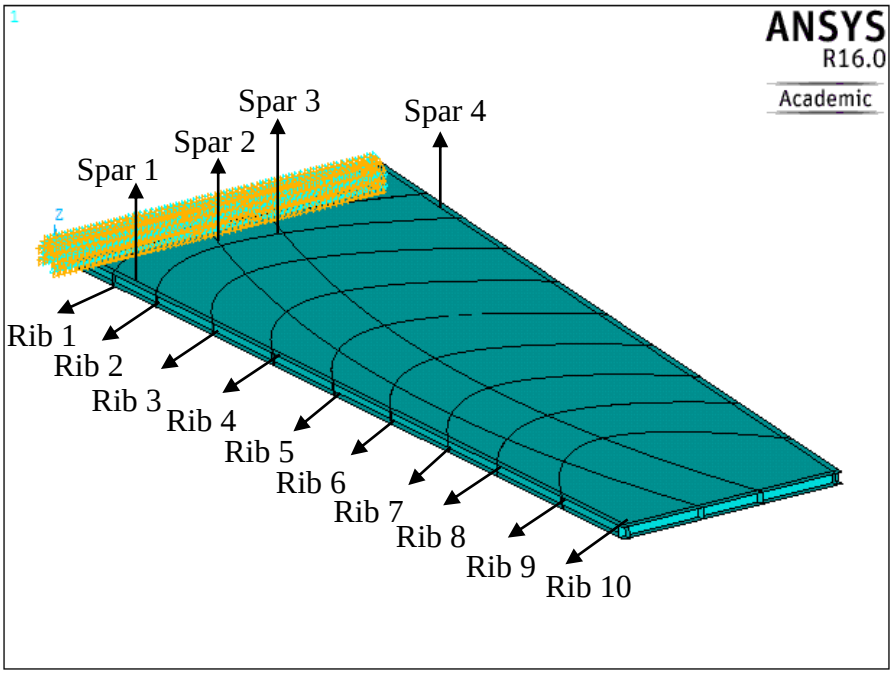

Figure 3.17 Top view of a wing box with tapered T.E. and curvilinear spars and ribs

Table 3.30 shows the natural frequencies and mode shapes of the tapered wing of this section, and a good correlation between the present study and the ANSYS® model is achieved verifying the present formulation.

Table 3.29 Coordinates of three points of the spars and ribs in Figure 3.17

Spar or Rib	**Point**	**X (mm)**	**Y (mm)**	**Spar or Rib**	**Point**	**X (mm)**	**Y (mm)**
	1	0	30		1	1651	0
Spar 1	2	2147	30	Rib 4	2	1194	500
	3	4293	30		3	1651	1423

Spar or Rib	Point	X (mm)	Y (mm)	Spar or Rib	Point	X (mm)	Y (mm)
	1	0	700		1	2108	0
Spar 2	2	2147	200	Rib 5	2	1651	500
	3	4293	400		3	2108	1364
	1	0	1000		1	2540	0
Spar 3	2	2147	500	Rib 6	2	2108	500
	3	4293	700		3	2540	1310
	1	0	1596		1	2972	0
Spar 4	2	2147	1329	Rib 7	2	2540	500
	3	4293	1061		3	2972	1256
	1	432	0		1	3340	0
Rib 1	2	200	500	Rib 8	2	2972	500
	3	432	1573		3	3340	1210
	1	762	0		1	3835	0
Rib 2	2	432	500	Rib 9	2	3340	500
	3	762	1531		3	3835	1149
	1	1194	0		1	4260	0
Rib 3	2	762	500	Rib 10	2	4260	500
	3	1194	1478		3	4260	1096

Table 3.30 First four modes of vibration of a tapered wing box with curvilinear spars and ribs

Present	ANSYS®	% Error
Mode 1, $\omega = 3.79$	Mode 1, $\omega = 3.77$	0.53
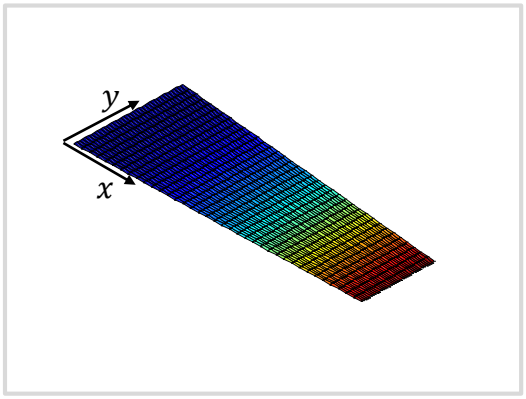	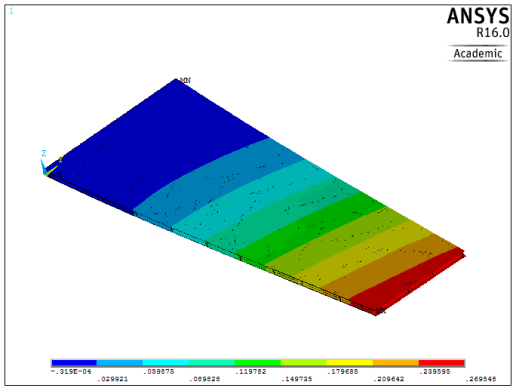	
Mode 2, $\omega = 18.26$	Mode 2, $\omega = 20.91$	12.67
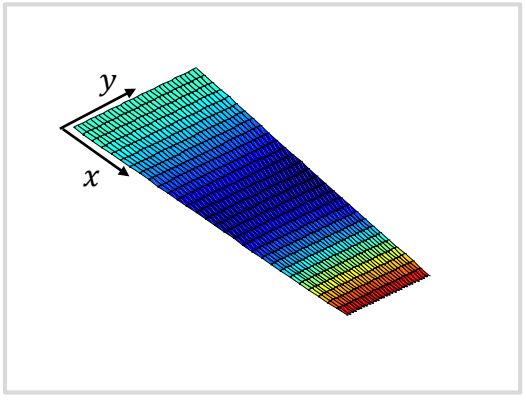	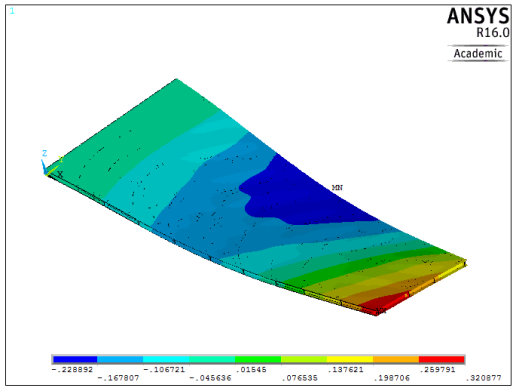	
Mode 3, $\omega = 30.90$	Mode 3, $\omega = 26.90$	14.87

Present	ANSYS®	% Error
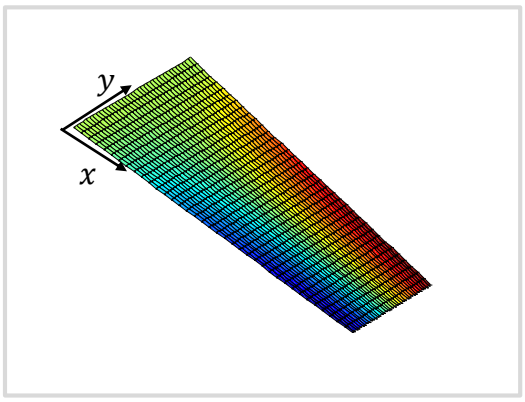	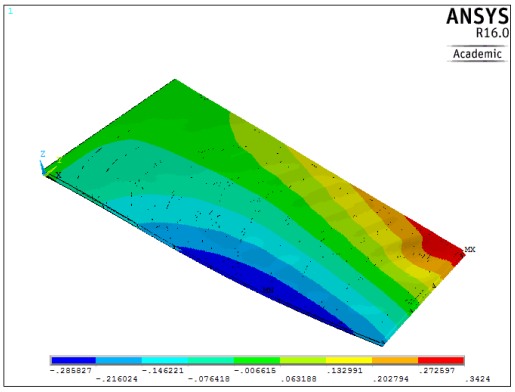	
Mode 4, $\omega = 50.89$	Mode 4, $\omega = 50.60$	0.57
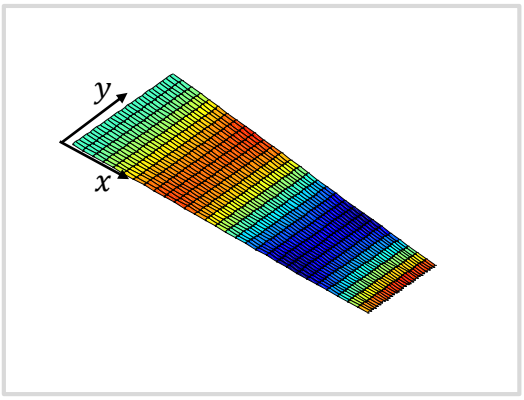	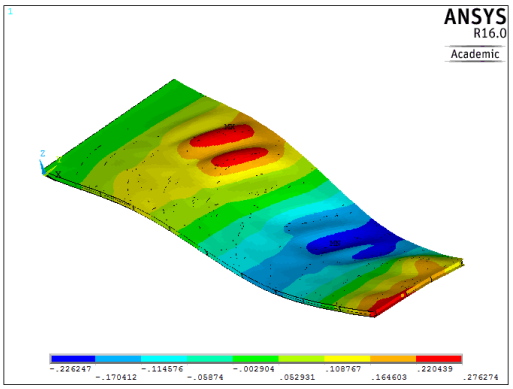	

4. Conclusion

The free vibration analysis of laminated composite stiffened plates and flutter analysis of isotropic and laminated unstiffened and straight-stiffened plates are carried out to validate the present formulation. The formulation is validated upon comparison with previous publications and ANSYS® models. The flutter analysis of laminated composite curvilinear stiffened plates is performed to assess the effects of the fiber angle and stiffener orientation on flutter of rectangular and skew plates under supersonic speeds. The results indicate that flutter can be passively controlled by changing the stiffener and the fiber orientations. However, there is a correlation between the skew angle and the stiffener and fiber orientation, and these factors must be designed simultaneously.

Three wing boxes with curvilinear spars and ribs are modeled using an equivalent plate model. The Ritz method and first order shear deformation theory is used in this study. The natural frequencies of the wing boxes from this study are compared with ANSYS® models, proving that the proposed plate model can accurately simulate the free vibration of a wing.

5. Recommendations

Although the results obtained in this study are satisfactory, there are some considerations that would certainly enrich the present research. First of all, the proposed method has some limitations regarding the wing thickness-to-chord ratio. To take care of this restriction and further refine the model, a high shear deformation theory (HSDT) could perhaps be considered. Replacing the plate formulation by shells and considering a cambered airfoil would also be a valuable improvement.

A more practical model could be considered in future studies. To elaborate, a more representative model of a tapered and swept wing with control surfaces, more internal details, such as spar and rib caps and stringers, could be investigated to obtain a better insight into the benefits of the proposed study. A greater variety of laminates such as unsymmetrical composite laminates should be studied.

The study of vibration of stiffened structures in general, is a prospective topic as it finds a lot of application in aerospace and other industries as previously mentioned. Therefore, the flutter analysis introduced in this report could be extended to wing boxes by using a subsonic method such as the Doublet Lattice Method (DLM). An obvious step after this research would be the optimization of the design considering flutter and static constraints. Optimization would be useful to evaluate the advantages of the proposed model over finite element models.

REFERENCES

Alyanak, E. J., & Pendleton, E. (2014). A design study employing aeroelastic tailoring and an active aeroelastic wing design approach on a tailless lambda wing configuration. *15th AIAA/ISSMO Multidisciplinary Analysis and Optimization Conference*, Atlanta, GA. June 16–20.

Carrera, E., Petrolo, M., & Varello, A. (2012). Advanced beam formulations for free-vibration analysis of conventional and joined wings. *Journal of Aerospace Engineering, 25(2)*, 282-293.

Chen, P. C., Jha, R., Sarhaddi, D., Liu, D. D., Griffin, K., & Yurkovich, R. (2000). A variable stiffness spar (VSS) approach for aircraft maneuver enhancement using ASTROS. *Journal of Aircraft, 37(5)*, 865–871.

Chowdary, T. V., Sinha, P. K., & Parthan, S. (1996). Finite element flutter analysis of composite skew panels. *Computers and Structures, 58(3)*, 613-620.

Dang, T. D., Kapania, R. K., Slemp, W. C. H., Bhatia, M., & Gurav, S. P. (2010). Optimization and postbuckling analysis of curvilinear-stiffened panels under multiple-load cases. *Journal of Aircraft, 47(5)*, 1656-1671.

Flutter. (2005). In *An Illustrated Dictionary of Aviation*.

Forster, E. E., & Yang, H. T. (1998). Flutter control of wing boxes using piezoelectric actuators. *Journal of Aircraft, 35(6)*, 949-957.

Hirschel, E. H., Prem, H. & Madelung, G. (2003). *Aeronautical research in Germany – from Lilienthal until today*. Springer, Berlin, London.

Hwu, C., & Tsai, A. S. (2002). Aeroelastic divergence of stiffened composite multicell wing structures. *Journal of Aircraft, 39(2)*, 242-251.

Kapania, R. K., & Liu, Y. (2000). Static and vibration analyses of general wing structures using equivalent plate models. *AIAA Journal, 28(7)*, 1269-1277.

Kapania, R. K, Li, J., & Kapoor, H. (2005). Optimal design of unitized panels with curvilinear stiffeners. *AIAA 5th ATIO and the AIAA 16th Lighter-than-Air Systems Technology Conference and Balloon Systems Conference*, Arlington, VA, September 26-28.

Kolli, M., & Chandrashekhara, K. (1997). Non-linear static and dynamic analysis of stiffened laminated plates. *International Journal of Non-Linear Mechanics, 32(1)*, 89-101.

Koo, K. N., & Hwang, W. S. (2004). Effects of hysteretic and aerodynamic damping on supersonic panel flutter of composite plates. *Journal of Sound and Vibration, 273(3)*, 569-583.

Liao, C. L., & Sun, Y. W. (1993). Flutter analysis of stiffened laminated composite plates and shells in supersonic flow. *AIAA Journal, 31(10)*, 1897-1905.

Librescu, L., Marzocca, P., & Silva, W. A. (2002). Supersonic/hypersonic flutter and postflutter of geometrically imperfect circular cylindrical panels. *Journal of Spacecraft and Rockets, 39(5)*, 802-812.

Liew, K., Xiang, Y., Kitipornchai, S., & Lim, M. (1994). Vibration of rectangular Mindlin plates with intermediate stiffeners. *Journal of Vibration and Acoustics, 116*, 529-535.

Locatelli, D., Mulani, S. B., Liu, Q., Tamijani, A. Y., & Kapania, R. K. (2014). Supersonic wing optimization using SpaRibs. *NASA*.

Lopes, C. S., Gürdal, Z., & Camanho, P. P. (2008). Variable-stiffness composite panels: buckling and first-ply failure improvements over straight-fiber laminates. *Computers & Structures, 86(9)*, 897–907.

Lovejoy, A. E. (1994). Natural frequencies and an atlas of mode shapes for generally-laminated, thick, skew, trapezoidal plates. Master Thesis, Aerospace and Ocean Dept., Virginia Polytechnic Institute and State University, Blacksburg, VA.

Moosavi, M. R., Oskouei, A. N., & Khelil, A. (2005). Flutter of subsonic wing. *Thin-Walled Structures, 43(4)*, 617-627.

Mulani, S. B., Locatelli, D., & Kapania, R. K. (2011). Grid-stiffened panel optimization using curvilinear stiffeners. *52nd AIAA/ASME/ASCE/AHS/ASC Structures, Structural dynamics and Materials Conference*. Denver, CO, April 4-7.

Peng, S., Kapania, R. K., & Dong, C. Y. (2015). Vibration and buckling analysis of curvilinearly stiffened plates using finite element method. *AIAA Journal, 53(5)*, 1319-1335.

Prusty, B. G., Ray, C., & Satsangi, S.K. (2001). First ply failure analysis of stiffened panels – a finite element approach. *Composite Structures, 51*, 73-81.

Singha, M. K., & Ganapathi, M. (2005). A parametric study on supersonic flutter behavior of laminated composite skew flat panels. *Composite Structures, 69(1)*, 55-63.

Stanford, B., Beran, P., & Bhatia, M. (2014). Aeroelastic topology optimization of blade-stiffened panels. *Journal of Aircraft, 51(3)*, 938-944.

Tamijani, A. Y., & Kapania, R. K. (2010). Vibration of plate with curvilinear stiffeners using meshfree method. *AIAA Journal, 48(8),* 1569-1581.

Tamijani, A. Y., McQuigg, T., & Kapania, R. K. (2010). Free vibration analysis of curvilinear-stiffened plates and experimental validation. *Journal of Aircraft, 47(1),* 192-200.

Tamijani, A. Y., Mulani, S. B., & Kapania, R. K. (2014). A framework combining meshfree analysis and adaptive kriging for optimization of stiffened panels. *Structural and Multidisciplinary Optimization, 49*, 577-594.

Ventres, C. S., & Dowell, E. H. (1970). Comparison of theory and experiment for nonlinear flutter of loaded plates. *AIAA Journal, 8(11),* 2022-2030.

Vepa, R. (2008). Aeroelastic analysis of wing structures using equivalent plate models. *AIAA Journal, 46(5),* 1216-1225.

Vinson, J. R., & Sierakowsko, R. L. (2002). The Behavior of Structures Composed of Composite Materials. Kluwer Academic Publisher, NY.

Vlachoutsis, S. (1992). Shear correction factors for plates and shells. *International Journal for Numerical Methods in Engineering, 33,* 1537-1552.

Wright, J. R., & Cooper, J. E. (2007). *Introduction to aircraft aeroelasticity and loads*. Hoboken, NJ: John Wiley

Zhao, H., & Cao, D. (2013). A study on the aero-elastic flutter of stiffened laminated composite panel in the supersonic flow. *Journal of Sound and Vibration, 332(19),* 4668-4679.

Zhao, W., & Kapania, R. (2016). Buckling analysis of unitized curvilinearly stiffened composite panels. *Composite Structures, 135,* 365-382.